TKK Dissertations 230
Espoo 2010

DATA-ANALYSIS PERSPECTIVES ON NATURALISTIC STIMULATION IN FUNCTIONAL MAGNETIC RESONANCE IMAGING

Doctoral Dissertation

Sanna Malinen

Aalto University
School of Science and Technology
Low Temperature Laboratory
Brain Research Unit

TKK Dissertations 230
Espoo 2010

DATA-ANALYSIS PERSPECTIVES ON NATURALISTIC STIMULATION IN FUNCTIONAL MAGNETIC RESONANCE IMAGING

Doctoral Dissertation

Sanna Malinen

Doctoral dissertation for the degree of Doctor of Science in Technology to be presented with due permission of the Faculty of Information and Natural Sciences for public examination and debate in Auditorium TU1 at the Aalto University School of Science and Technology (Espoo, Finland) on the 11th of June 2010 at 12 noon.

Aalto University
School of Science and Technology
Low Temperature Laboratory
Brain Research Unit

Aalto-yliopisto
Teknillinen korkeakoulu
Kylmälaboratorio
Aivotutkimusyksikkö

Aalto University
School of Science and Technology
Faculty of Information and Natural Sciences
Department of Biomedical Engineering and Computational Science

Aalto-yliopisto
Teknillinen korkeakoulu
Informaatio- ja luonnontieteiden tiedekunta
Lääketieteellisen tekniikan ja laskennallisen tieteen laitos

Distribution:
Aalto University
School of Science and Technology
Low Temperature Laboratory
Brain Research Unit
P.O. Box 15100
FI - 00076 Aalto
FINLAND
URL: http://ltl.tkk.fi/
Tel. +358-9-470 25619
Fax +358-9-470 22969
E-mail: sanna.malinen@tkk.fi

ISBN 978-952-60-3207-8
ISBN 978-952-60-3208-5 (PDF)
ISSN 1795-2239
ISSN 1795-4584 (PDF)
URL: http://lib.tkk.fi/Diss/2010/isbn9789526032085/

TKK-DISS-2774

Multiprint Oy
Espoo 2010

Aalto University

ABSTRACT OF DOCTORAL DISSERTATION	AALTO UNIVERSITY SCHOOL OF SCIENCE AND TECHNOLOGY P.O. BOX 11000, FI-00076 AALTO http://www.aalto.fi

Author Sanna Malinen

Name of the dissertation
Data-analysis perspectives on naturalistic stimulation in functional magnetic resonance imaging

Manuscript submitted March 9, 2010	Manuscript revised May 24, 2010

Date of the defence June 11, 2010

☐ Monograph ☒ Article dissertation (summary + original articles)

Faculty Information and Natural Sciences
Department Biomedical Engineering and Computational Science
Field of research Engineering Physics, Biomedical Engineering
Opponent(s) Prof. Vince Calhoun
Supervisor Prof. Risto Ilmoniemi
Instructor Acad. Prof. Riitta Hari

Abstract

Modern brain imaging allows to study human brain function during naturalistic stimulus conditions, which entail specific challenges for the analysis of the brain signals. The conventional analysis of data obtained by functional magnetic resonance imaging (fMRI) is based on user-specified models of the temporal behavior of the signals (general linear model, GLM). Alongside these approaches, data-based methods can be applied to model the signal behavior either on the basis of the measured data, as in seed-point correlations or inter-subject correlations (ISC), or alternatively the temporal behavior is not modeled, but spatial signal sources and related time courses are estimated directly from the measured data (independent component analysis, ICA).

In this Thesis, fMRI data-analysis methods were studied and compared in experiments that gradually proceeded towards more naturalistic and complex stimuli. ICA showed superior performance compared with GLM-based method in the analysis of naturalistic situations. The particular strengths of the ICA were its capability to reveal activations when signal behavior deviated from an expected model, and to show similarities between signals of different brain areas and of different individuals.

The practical difficulty of ICA in naturalistic conditions is that the user may not be able to determine, purely on the basis of the components' spatial distribution or temporal behavior, the brain networks that are related to the given stimuli. In this Thesis, a new solution to sort the components was proposed that ordered the components according to the ISC map, and thereby facilitated the selection of stimulus-related components. The method prioritized brain areas closely related to sensory processing, but it also revealed circuitries of intrinsic processing if they were affected similarly across individuals by external stimulation.

Analysis issues related to the impact of physiological noise in fMRI signals were also considered. Cardiac-triggered fMRI improved detection of touch-related activation both in the thalamus and in the secondary somatosensory cortex. The most common way to eliminate noise is to filter the data. In this Thesis, however, aberrations in temporal behavior, as well as in functional connectivities in chronic pain patients were observed, which likely could not have been revealed with conventional temporal filtering.

Keywords functional magnetic resonance imaging, statistical parametric mapping, independent component analysis, correlation analysis, brain

ISBN (printed) 978-952-60-3207-8	ISSN (printed) 1795-2239
ISBN (pdf) 978-952-60-3208-5	ISSN (pdf) 1795-4584
Language English	Number of pages 58 + 46 in appendices

Publisher Low Temperature Laboratory, Aalto University of Science and Technology

Print distribution Low Temperature Laboratory, Aalto University of Science and Technology

☒ The dissertation can be read at http://lib.tkk.fi/Diss/2010/isbn9789526032085/

Aalto-yliopisto

VÄITÖSKIRJAN TIIVISTELMÄ	AALTO-YLIOPISTO TEKNILLINEN KORKEAKOULU PL 11000, 00076 AALTO http://www.aalto.fi

Tekijä Sanna Malinen

Väitöskirjan nimi
Toiminnallisen magneettikuvauksen data-analyysimenetelmiä luonnonmukaisissa koetilanteissa

Käsikirjoituksen päivämäärä 9.3.2010	Korjatun käsikirjoituksen päivämäärä 24.5.2010
Väitöstilaisuuden ajankohta 11.6.2010	
☐ Monografia	☒ Yhdistelmäväitöskirja (yhteenveto + erillisartikkelit)

Tiedekunta	Informaatio- ja luonnontieteiden tiedekunta
Laitos	Lääketieteellisen tekniikan ja laskennallisen tieteen laitos
Tutkimusala	Teknillinen fysiikka, lääketieteellinen tekniikka
Vastaväittäjä(t)	Prof. Vince Calhoun
Työn valvoja	Prof. Risto Ilmoniemi
Työn ohjaaja	Akat. prof. Riitta Hari

Tiivistelmä

Modernin aivokuvantamisen mahdollisuus tutkia aivotoimintaa luonnonmukaisissa tilanteissa asettaa erityisiä vaatimuksia aivoista mitattujen signaalien käsittelyyn. Perinteiset toiminnallisen magneettikuvauksen (fMRI) data-analyysimenetelmät ovat perustuneet signaalien aikakäyttäytymisen malleihin (yleinen lineaarinen malli, GLM). Näiden rinnalle tarvitaan datalähtöisiä menetelmiä, joissa malli signaalinmuutoksille saadaan joko mitatusta datasta itsestään (esim. lähdealuekorrelaatiot tai koehenkilöiden väliset korrelaatiokartat, ISC) tai vaihtoehtoisesti aikakäyttäytymistä ei mallinneta, vaan signaalilähteet lasketaan suoraan mitatusta datasta (riippumattomien komponenttien analyysi, ICA).

Tässä väitöskirjassa tutkittiin ja vertailtiin fMRI-data-analyysimenetelmiä koeasetelmissa, joissa edettiin asteittain kohti luonnonmukaisempia ja monimutkaisempia ärsykkeitä. ICA:n havaittiin sopivan GLM-menetelmää paremmin luonnonmukaisten ärsykkeiden analyysiin. ICA:n erityisenä vahvuutena oli kyky löytää aktivaatioita tilanteissa, joissa signaalin aikakäytös poikkesi ennakoidusta. Lisäksi ICA paljasti signaalien samankaltaisuudet sekä eri aivoalueiden että koehenkilöiden välillä.

ICA:n käytännön ongelma luonnonmukaisissa tilanteissa on, etteivät ärsykkeeseen liittyvät aivoverkostot välttämättä erotu signaalin paikkajakauman tai aikakäyttäytymisen perusteella. Väitöskirjassa esitettiin ratkaisuksi komponenttien järjestäminen ISC-kartan perusteella, mikä helpotti ärsykesidonnaisten komponenttien valintaa. ISC-pohjainen järjestely suosi aistitiedon käsittelyyn kiinteimmin osallistuvia aivoalueita, mutta sillä löydettiin myös ns. lepoverkostoja, jos ärsykkeet muokkasivat niiden toimintaa samankaltaisesti eri koehenkilöillä.

Väitöskirjassa käsiteltiin myös fysiologisen kohinan vaikutusta fMRI-signaaliin. Sydämen toimintaan tahdistettu magneettikuvaus paransi tuntoärsykkeiden aikaansaamien aktivaatioiden havaitsemista talamuksessa ja sekundaarisella tuntoaivokuorella. Tavallisimmin fysiologisen kohinan vaikutusta vähennetään suodattamalla. Väitöskirjassa todettiin kuitenkin kroonisilla kipupotilailla poikkeamia sellaisessa signaalien ajallisessa käytöksessä ja aivojen toiminnallisissa yhteyksissä, jotka olisivat perinteisillä suodatustavoilla saattaneet jäädä havaitsematta.

Asiasanat toiminnalinen magneettikuvaus, tilastollinen parametrikartoitus, riippumattomien komponenttien analyysi, korrelaatioanalyysi, aivot

ISBN (painettu)	978-952-60-3207-8	ISSN (painettu)	1795-2239
ISBN (pdf)	978-952-60-3208-5	ISSN (pdf)	1795-4584
Kieli	englanti	Sivumäärä	58 + 46 liitteinä

Julkaisija Kylmälaboratorio, Aalto-yliopiston teknillinen korkeakoulu

Painetun väitöskirjan jakelu Kylmälaboratorio, Aalto-yliopiston teknillinen korkeakoulu

☒ Luettavissa verkossa osoitteessa http://lib.tkk.fi/Diss/2010/isbn9789526032085/

Academic dissertation

Data-analysis perspectives on naturalistic stimulation in functional magnetic resonance imaging

Author

Sanna Malinen
Brain Research Unit
and Advanced Magnetic Imaging Centre
Low Temperature Laboratory
Aalto University of Science and Technology
Finland

Supervisor

Professor Risto Ilmoniemi
Department of Biomedical Engineering
and Computational Science
Aalto University of Science and Technology
Finland

Instructor

Academy Professor Riitta Hari
Brain Research Unit,
Low Temperature Laboratory
Aalto University of Science and Technology
Finland

Preliminary examiners

Associate Professor Elia Formisano
Faculty of Psychology and Neurosciences
Department of Cognitive Neuroscience
Maastricht University
The Netherlands

Professor Aapo Hyvärinen
Department of Mathematics and Statistics
and Department of Computer Science
University of Helsinki
Finland

Official opponent

Professor Vince Calhoun
The Mind Research Network
University of New Mexico
USA

Table of contents

List of publications

This Thesis is based on four publications, referred to in the text as Studies 1–4.

1. Malinen S, Schürmann M, Hlushchuk Y and Hari R (2006). Improved differentiation of tactile activations in human secondary somatosensory cortex and thalamus using cardiac-triggered fMRI. Experimental Brain Research 174:297–303.

2. **Malinen S**, Hlushchuk Y and Hari R (2007). Towards natural stimulation in fMRI—issues of data analysis. NeuroImage 35:131–139.

3. **Malinen S** and Hari R (2010). Comprehension of audiovisual speech: Data-based sorting of independent components of fMRI activity. TKK Report, TKK-KYL-023.

4. **Malinen S**, Vartiainen N, Hlushchuk Y, Koskinen M, Ramkumar P, Forss N, Kalso E and Hari R (2010). Aberrant temporal and spatial brain activity during rest in patients with chronic pain. Proceedings of the National Academy of Sciences U S A 107:6493–6497.

Contribution of the author

I had an active role at all stages of research of this Thesis, although the studies are a result of group effort. I participated in the planning phase of each study. I had the main responsibility for the fMRI measurements in Studies 1–3, and I participated in collecting fMRI data for Study 4. For Study 2, I created the stimulus material, and for Study 3, I edited the video stimuli. In all studies, I carried out the fMRI analysis (excluding correlation between fMRI signals and ECG and respiration in Study 4); the analysis included, beyond conventional procedures, the implementation of analysis algorithms for cardiac-triggered image correction, inter-subject correlation studies, and related calculations. I proposed and implemented a new combination of two existing data-driven methods in Study 3 to sort independent components in naturalistic and continuous stimulus conditions. As the first author of all manuscripts, I had the main responsibility for writing the publications, with active participation of the co-authors.

Abbreviations

ACC	Anterior cingulate cortex
ACx	Auditory cortex
ANS	Autonomic nervous system
BOLD	Blood oxygen level dependent (signal)
fMRI	Functional magnetic resonance imaging
FOV	Field of view
GLM	General linear model
GRE	Gradient echo
HRF	Hemodynamic response function
IC	Independent component
ICA	Independent component analysis
IFG	Inferior frontal gyrus
IPL	Inferior parietal lobule
ISC	Inter-subject correlation
MNI	Montreal Neurological Institute (space)
MR	Magnetic resonance
MRI	Magnetic resonance imaging
MTG	Middle temporal gyrus
NMR	Nuclear magnetic resonance
POS	Parieto-occipital sulcus
RAI	Right anterior insula
RF	Radio frequency
ROI	Region of interest
TD	Trigger delay
TE	Echo time
TR	Repetition time
TW	Trigger window
SI	Primary somatosensory cortex
SII	Secondary somatosensory cortex
SPM	Statistical parametric mapping
STD	Standard deviation
STS	Superior temporal sulcus
VisCx	Visual cortex
V1/V2	Early visual cortices
V5/MT	Motion-sensitive visual cortex

Acknowledgements

This Thesis was carried out at the Brain Research Unit (BRU) of the Low Temperature Laboratory (LTL) and at the Advanced Magnetic Imaging Centre (AMI) of the Aalto University of Science and Technology. My work was financially supported by the Academy of Finland (National Centers of Excellence program, and NEURO research grant), Finnish Graduate School of Neuroscience (FGSN), Research Foundation of Helsinki University of Technology, Finnish Foundation of Technology Promotion, Jenny and Antti Wihuri Foundation and Emil Aaltonen Foundation.

It has been an honor to do research at the BRU and LTL, in a qualified scientific environment led by Prof. Mikko Paalanen. I have been privileged to work under the most skillful and insightful supervision of the director of the BRU, Acad. Prof. Riitta Hari. I express my deepest gratitude to her for the inspiring and devoted guidance of this Thesis. My sincere thanks go also to collaborators Nina Forss, Yevhen Hluschuck, Eija Kalso, Miika Koskinen, Pavan Ramkumar, Martin Schürmann and Nuutti Vartiainen. I also want to thank Maarit Aro for collaboration in studies related to this Thesis. It has been a pleasure to work with all of you.

I would like to thank my supervising professor Risto Ilmoniemi for his contribution in the writing process and finalizing of this Thesis. My sincere thanks go to the reviewers of this Thesis, Ass. Prof. Elia Formisano and Prof. Aapo Hyvärinen, for their effort and insightful comments. I would also like to thank Cathy Nangini for language corrections.

I am grateful to the members of the follow-up group of FGSN, Prof. Samuel Kaski and Prof. Pekka Meriläinen for our annual appointments, your interest, ideas and affirmative attitude towards the ongoing research.

Most of the work for this Thesis was carried out in the AMI Centre and I want to thank the people there for their contribution in various forms. I would like to thank Ville Renvall for comments and discussions related to MRI physics. Jaana Hiltunen, Marita Kattelus, Antti Tarkiainen, and Simo Vanni, thank you for your help with several scientific or practical issues.

I am thankful to the computer support team of AMI and BRU, and I also want to thank the secretaries and other support team for the help with several practical matters.

I want to express my gratitude to the whole BRU group, the present and former members of it, with whom I have worked or shared the coffee breaks during the graduate studies. It has been pleasant to do research in such an environment full of intelligent eager minds. Especially, I want to thank the three wonderful ladies, Linda Stenbacka, Miiu Kujala and Annika Hultén for friendship and great company both at work and outside the laboratory.

I am deeply grateful to my parents and to my sister Anne and her family. Your invaluable support and encouragement have carried me throughout my life. I also want to thank the Malinen family for their kindness and care whenever we have spent time together.

My warmest hugs and thanks belong to my family, to my dear husband Arto and our cute little son Atte. You are my everything.

Introduction

We live in a constantly changing world where we see, hear, touch, smell, taste, and move more or less continuously. Until the past few years, however, functional brain imaging has relied on, or even been chained to, very simplistic artificial laboratory environments that only weakly resemble the real environment we live in. During a conventional functional magnetic resonance imaging (fMRI) experiment, stimulus blocks of several seconds in duration alternate with rest or baseline periods. Although these simple stimulation setups still have their firm place in the study of different brain systems, we are not able to fully understand human brain function in isolation from its real environment. That is why one of the current challenges of functional brain imaging is to move towards more naturalistic experimental setups. Moreover, naturalistic stimuli can activate, in a specific manner, more brain areas than conventional stimulus settings (Bartels and Zeki, 2004).

Naturalistic conditions introduce, however, enormous challenges for brain research. First, how to create in a laboratory a stimulus environment that sufficiently resembles real-life situations? Second, how to analyze the complex brain responses elicited by naturalistic and continuously-varying stimulation?

In laboratory, the improvements of scanner environments have been essential for the collection of high-quality functional-brain-imaging data, since the inherent signal-to-noise ratio of fMRI signal is rather poor. Scanners with high magnetic field strengths (typically 3–7 T in research use) now allow the collection of fine-resolution functional images rather rapidly or with better signal-to-noise ratio compared with lower magnetic field strengths.

The fMRI scanner, however, imposes limitations on stimulus presentation, and it is difficult to create real-life-like conditions in the narrow scanner bore. It is, however, possible to mimic reality by, for example, using video stimuli that provide a replicable and nearly realistic presentation of our natural environment.

From the data-analysis point of view, a video stimulus is very complex compared with conventional simplistic stimuli presented in blocks of several seconds in an on–off manner. Data analysis of such “block-design fMRI” typically relies on pre-determined models of brain responses, time-locked to discrete stimulus presentation. During naturalistic and continuous stimulation, however, brain responses are much more complex, and this difficulty compels data analysis away from the traditional model-based approaches towards more data-driven methods.

This Thesis concentrates on certain aspects of data-analysis methods required in the analysis of brain responses under naturalistic stimulation conditions. The performed fMRI experiments proceed gradually from conventional fMRI block designs towards more complex and continuous stimulus set-ups. In Study 1, tactile stimulation was presented in a traditional

block design. In Studies 2 and 3, more complex multi-sensory stimulation was presented; in Study 2, videos, as well as tactile and auditory stimuli, were presented in separate blocks, but the unimodal stimulation was always on, with no separate rest periods between the blocks. Continuous audio-visual speech, with simultaneous auditory and visual information, was presented in Study 3. In Study 4, subjects were measured during resting state without external stimulation; one group of subjects suffered from chronic pain, and thus their "stimuli" emerged intrinsically because of the continuous pain they experienced.

The data-analysis methods of this Thesis extend from general-linear-model (GLM) based statistical parametric mapping (SPM) to data-driven independent component analysis (ICA) and correlation methods. In Study 1, only GLM was utilized to analyze the simple block design. Study 2 demonstrated the superiority of ICA compared with GLM in separating signals related to, *e.g.*, speech *vs.* tone pips, or processing of visual motion *vs.* more static images.

ICA conveniently depicts those functionally connected brain areas that show common temporal variation. One challenge in ICA is, however, to separate the stimulus-related independent components (ICs) from ICs related to, *e.g.*, intrinsic brain activity that does not depend on external stimulation or various types of artifacts. Study 3 presents a new approach, which facilitates the IC sorting by pre-mapping all activated brain areas in the form of an inter-subject correlation map. In Study 4, both ICA and seed-point correlations were used to demonstrate altered functional connectivity of the affective pain matrix in patients suffering from chronic pain.

Some physiological factors that can affect the measured blood oxygen level dependent (BOLD) signal are also discussed in this Thesis. In Study 1, the effect of cardiac pulsation was eliminated from the measured signal, and in Study 4, the discussion about possible effects of cardiac pulsations was revisited. Importantly, the frequency analysis of spontaneous fluctuations of brain activity in Study 4 provides insights into fMRI data filtering, suggesting that reducing physiological contamination by filtering the data may sometimes mask or remove effects of interest.

This Thesis summary consists of five parts. Chapter 1 presents the methodological background: the basic principles of functional magnetic resonance imaging and, more importantly, the analysis methods required to obtain statistically significant results from the measured fMRI data. Chapter 2 describes the aims of Studies 1–4 constituting this Thesis, and Chapter 3 explains the details and parameters of the particular methods applied. Chapter 4 presents the individual studies in more detail, their main findings, and conclusions. Finally, the discussion in Chapter 5 summarizes the general findings and provides some considerations on data-analysis methods as well as brief insights into future fMRI research involving naturalistic stimuli.

1 Background

1.1 Magnetic resonance imaging

Magnetic resonance imaging (MRI) is a technique to obtain high-resolution images from an object of interest by utilizing the magnetic properties of the sample and its interactions with external magnetic fields. MRI is based on the physical phenomenon called nuclear magnetic resonance (NMR).

The first NMR experiments were carried out in 1946 by two research groups, those of Felix Bloch (1946) and Edward Purcell (1946). Later, Raymond Damadian (1971) found out that NMR signal properties are specific for different types of tissues. Important advances in MR image collection were presented by Paul Lauterbur (1973), who introduced the field gradients for formation of magnetic resonance (MR) images, and by Peter Mansfield (1977), who developed echo planar imaging (EPI) as a technique for rapid image acquisition.

In the beginning of the 1990s, Seiji Ogawa and coworkers (1990) discovered the blood oxygen level dependent (BOLD) signal, thereby launching the era of fMRI. The discovery of the BOLD effect enabled studies on brain function. Compared with injected contrast agents, such as gadolinium (Belliveau et al., 1990, 1991), BOLD effect can be considered as an inherent contrast mechanism of the brain. BOLD was first observed in anesthetized rodents and was soon demonstrated also in humans (Bandettini et al., 1992; Frahm et al., 1992; Kwong et al., 1992; Ogawa et al., 1992).

Nowadays, MRI is a widely-used technique both in clinical use and in several branches of research. Its popularity is based on good spatial resolution and the versatility of the technique: a multitude of contrasts between different tissues can be obtained by an appropriate manipulation of certain imaging parameters.

Nuclear magnetic resonance

Nuclei with a non-zero spin quantum number, *i.e.,* with a net spin, interact with external magnetic fields. In a magnetic field of strength B_0 (here along z axis), the nuclei precess about the field at the Larmor frequency ω_0, which is proportional to the external magnetic field strength: $\omega_0 = \gamma B_0$, where γ is the nucleus-specific gyromagnetic ratio (Haacke et al., 1999). The most commonly used nucleus in MRI is hydrogen (a single proton) due to its abundance in living tissues. For hydrogen protons, $\gamma/2\pi$ = 42.58 MHz/T, and at 3-T magnetic field, ω_0 = 127.74 MHz, which is in the radio-frequency (RF) range of the electromagnetic spectrum.

Since the spin quantum number of a proton is ½, the energy levels of protons split in the external magnetic field into two states (Zeeman effect), and protons are then slightly more likely to populate the lower-energy state. The population difference of spins in the two energy states leads to an equilibrium magnetization M_0, which can also be considered as a classical

magnetization vector. The total energy difference between the two states of the proton is $\Delta E = \gamma B_0 \hbar = \omega_0 \hbar$, where $\hbar$ is the Planck's constant $h/2\pi$. Hence, a system of protons can absorb and emit energy at the Larmor frequency ω_0.

Because protons in the lower energy state can absorb energy ΔE, magnetization M_0 can be deviated from equilibrium by an additional magnetic field B_1 that is an RF pulse at the Larmor frequency. The deviation form the original orientation is described with flip angle α, modulated both by the amplitude and duration of B_1 (Buxton, 2009).

After RF excitation, magnetization gradually returns back to equilibrium, while a measurable NMR signal is emitted.

Relaxation and time constants

The dynamics of the relaxation of magnetization is characterized by the set of Bloch equations that in constant magnetic field can be written separately for the transverse M_x and M_y and longitudinal M_z (along the main field B_0) components of magnetization (Haacke et al., 1999)

$$\begin{aligned} \frac{dM_x}{dt} &= \gamma B_0 M_y - \frac{M_x}{T_2} \\ \frac{dM_y}{dt} &= -\gamma B_0 M_x - \frac{M_y}{T_2}, \\ \frac{dM_z}{dt} &= -\frac{M_0 - M_z}{T_1} \end{aligned} \qquad (1)$$

where T_1 and T_2 denote the longitudinal spin–lattice and transverse spin–spin relaxation time constants, respectively. Longitudinal relaxation results from the energy exchange between the spins and lattice, and T_1 relaxation evolves in time according to the exponential equation $M_z(t) = M_0(1 - e^{-t/T_1})$. The transverse relaxation T_2, related to the decay of transverse magnetization M_{xy}, occurs due to spin–spin interactions and is characterized by $M_{xy}(t) = M_{xy}(0)e^{-t/T_2}e^{-i\omega_0 t}$, where the term $e^{-i\omega_0 t}$ denotes the precession about field B_0.

The third important time constant is the apparent transverse relaxation time T_2^*, which accounts for both the thermodynamic T_2 effects and magnetic field inhomogeneities: $1/T_2^* = 1/T_2 + \gamma\pi\Delta B_0$, where ΔB_0 are the field variations across the sample. Thus, T_2^* is always shorter than T_2. T_2^* relaxation is important in BOLD imaging (discussed below), in which local field variations of intra- and extravascular spaces related to blood oxygenation are measured.

Field gradients and image acquisition

Spatial information is coded into the magnetic resonance signal by an additional magnetic field B_g, whose z-component varies along the gradient direction: the x-gradient field $B_g = G_x x$, y-gradient field $B_g = G_y y$ and z-gradient field $B_g = G_z z$.

The gradient along the main field axis, G_z, is used for slice selection. G_z causes linear variations in the Larmor frequency of the protons and their excitation energies in nearby locations. For a specified G_z, the center frequency and the bandwidth of the excitation RF pulse determine the location and the thickness of the imaging slice.

After the slice selection, frequency and phase information is encoded into the signal. In the presence of frequency-encoding gradient G_x, Larmor frequencies vary linearly as a function of x according to $\omega(x) = \omega_0 + \gamma G_x x$. When the field gradient G_y has been on for a time T_y, the different phase angles accumulate, and the signals collected after T_y will have y-dependent phase $\varphi(y) = \gamma G_y y T_y$, *i.e.,* the signal is phase-encoded. These alternations in the local resonant frequencies and phases are unique for each spatial location within the imaged sample. Therefore, it is possible with field gradients to divide the object into three-dimensional volume elements called voxels.

Generally, MRI can be considered as a collection of frequency-space data matrix (axes frequency and phase) points in so-called k-space (Ljunggren, 1983; Twieg, 1983). A spatial image is obtained by Fourier transformation of the k-space data. The way the k-space is sampled determines the image field of view (FOV) and resolution.

Signal echo

After the initial excitation, spins gradually loose their phase coherence. However, the signal can be re-intensified by generating a "signal echo". Two main ways to produce the echo are either to apply a refocusing RF pulse (spin echo, SE), or perform certain gradient operations (gradient echo, GRE). In spin-echo imaging, a refocusing 180º RF pulse is applied after the excitation RF pulse to rephase the spins. The signal echo is generated at echo time (TE) after the initial excitation RF pulse, when the refocusing RF pulse is sent at t = TE/2. The time between successive excitation RF pulses is called the repetition time (TR).

In GRE imaging, no refocusing RF pulses are applied, but the echo is generated by de- and rephasing the signal with the frequency-encoding gradient. A negative gradient introduces a spatially linear variation in the precession frequencies of the spins, thus dispersing their phase coherence. A subsequent positive gradient then reverses the spin phase dispersion and generates an echo.

GRE imaging is sensitive to T_2^* effects. Starting from the Bloch equations, and assuming that transverse magnetization is totally dephased after the preceding excitation pulse, the echo amplitude A in GRE imaging can be derived (Liang and Lauterbur, 2000)

$$A = M_0 e^{-\frac{\mathrm{TE}}{T_2^*}} \sin(\alpha) \frac{1 - e^{-\frac{\mathrm{TR}}{T_1}}}{1 - \cos(\alpha) e^{-\frac{\mathrm{TR}}{T_1}}} . \quad (2)$$

Generally, the measured MR signal depends both on the intrinsic properties of the tissues, such as proton density and relaxation time constants, as well as the parameters of the pulse sequence (such as TR, TE, and α), with which the magnetic resonance image is collected.

1.1.1 Functional imaging based on the BOLD effect

The magnetic properties of hemoglobin form the basis of the BOLD contrast in fMRI: oxygenated hemoglobin is diamagnetic and deoxygenated paramagnetic, and the changes in their relative amounts in an activated brain area can be seen in T_2^*-weighted MR images. Deoxygenated hemoglobin distorts the local field around the vessels, leading to a loss of the MR signal. In activated brain areas, the local oxygen metabolism slightly increases. However, more oxygen is available in the activated brain area than is consumed, and thus venous blood becomes more oxygenated. This leads to signal increase in fMRI images (Huettel et al., 2005; Buxton, 2009).

The BOLD effect is affected by changes related to neuronal activation, such as blood flow, blood volume, and the rate of O_2 metabolism. Thus, the BOLD signal is not a direct measure of neural activity, but correlates with it (Logothetis et al., 2001, 2002). The BOLD response reflects activity of a large group of adjacent neurons. With optical imaging it has been shown that the spread of oxygenated hemoglobin is wider than the spatial extent of the initial increase of deoxyhemoglobin, which more closely matches the location of neuronal activity at the onset of neuronal activity (Malonek and Grinvald, 1996).

Hemodynamic response function

Temporally, the BOLD response to a single stimulus event is rather slow compared with the electrical responses of neurons. After a stimulus event at $t = 0$, the BOLD response starts to increase after 2 s and peaks typically 5–6 s after the stimulus onset. The response vanishes completely after 25–30 s (Friston et al., 1998a). Sometimes the BOLD response also shows an initial dip (Menon et al., 1995; Malonek and Grinvald, 1996), which is seen particularly at higher field strengths.

The BOLD impulse response for a single stimulus event can be characterized by a hemodynamic response function (HRF), which can be modeled, *e.g.*, with gamma functions

(Friston et al., 1994; Boynton et al., 1996). Currently, the most commonly used model is the sum of two gamma functions (Friston et al., 1998a), which can be completed with temporal derivatives of the HRF (canonical HRF) (Friston et al., 1998b). Figure 1 presents the default shape of the HRF inbuilt in SPM2 software (http://www.fil.ion.ucl.ac.uk/spm/).

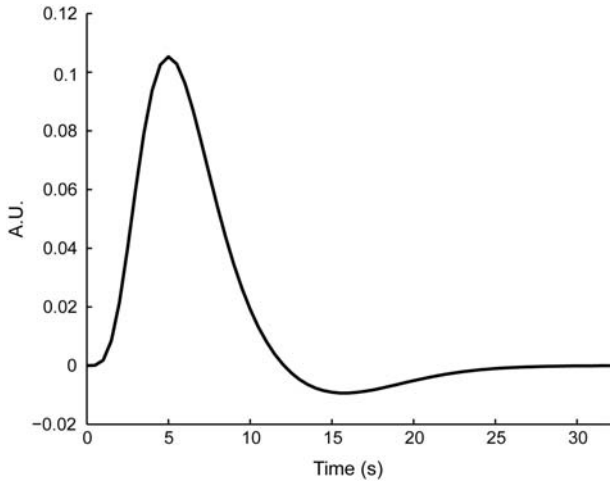

Figure 1. Hemodynamic response function (or BOLD impulse response) is a sum of two gamma functions (SPM2 default).

1.1.2 Physiological noise and its removal from fMRI signals

BOLD signals measured with fMRI can have several other sources of variation in addition to the hemodynamic changes related to neuronal activation. The main sources of noise in fMRI signal are *(i)* thermal noise, *(ii)* system noise arising from imaging hardware, and *(iii)* subject-related noise. Major components of the subject-related noise derive from head motion during the scanning and physiological pulsations, *e.g.,* due to cardiac and respiratory function. Physiological noise dominates the signal noise at 3 T (Krüger and Glover, 2001).

Head-motion correction is a standard preprocessing step in fMRI analysis (see *Realignment* in section 1.2.1). Other types of physiological noise can be suppressed, *e.g.,* with proper data filtering (Biswal et al., 1996), or by estimating and correcting for noise either in *k*-space (Hu et al., 1995) or in spatial images (Glover et al., 2000; Chuang and Chen, 2001). Artifacts have also been detected and removed with ICA (Thomas et al., 2002; Perlbarg et al., 2007). Moreover, physiological noise can be reduced by adapting the timing of image acquisition with the heart (or respiration) rate, and thereby removing the effects of pulsations from the functional images. Such an approach was used in Study 1 of this Thesis.

Cardiac-triggered imaging

To eliminate the effect of heart pulsations, fMRI image acquisition can be synchronized with the heart rate (cardiac-triggered fMRI). In these acquisitions, successive functional images are always collected in the same phase of the cardiac cycle. Cardiac-triggered image acquisition

has been used, *e.g.*, in studies of cortical and subcortical auditory areas (Guimaraes et al., 1998; Griffiths et al., 2001; Krumbholz et al., 2005; Zhang et al., 2006).

In cardiac-triggered imaging, an *effective TR* is determined by the time of the R–R interval and the number of successive R-peaks, during which one volume is collected (R refers to the most prominent electrocardiogram deflection, indicating contraction of the heart muscle). Before the collection of each volume can start, the fMRI scanner waits for the trigger signal (R peak) during a pre-set trigger window (TW), which is a user-defined percentage of the cardiac cycle time. After the trigger detection, the scanner waits for a trigger-delay (TD) time before the data collection starts.

In cardiac-triggered imaging, the TR is not constant, which leads to varying levels of T_1 relaxation of signals. These variations need to be corrected in post-acquisition image processing. The correction method (DuBois and Cohen, 2000) applied in this Thesis is based on a theoretical assumption of the GRE signal magnitude S, which is proportional to the signal echo presented in Equation (2). When signals from corresponding voxels are measured at two different TR values, TR_1 and TR_2, the ratio of the corresponding signal magnitudes S_1 and S_2 at $\alpha = 90^\circ$, is

$$\frac{S_1}{S_2} = \frac{1 - e^{-\mathrm{TR}_1/T_1}}{1 - e^{-\mathrm{TR}_2/T_1}}. \tag{3}$$

If the signal is totally recovered during the second acquisition, *i.e.,* $\mathrm{TR}_2 \approx \infty$, the T_1-value for a given voxel i can be obtained as

$$T_{1,i} = -\frac{\mathrm{TR}_1}{\ln(1 - S_{1,i}/S_{2,i})}, \tag{4}$$

and the corrected voxel intensity value at volume n

$$\hat{S}_{i,n} = S_{i,n} \frac{1 - e^{-\mathrm{TR}/T_{1,i}}}{1 - e^{-t_n/T_{1,i}}}, \tag{5}$$

where TR is the constant repetition time and $S_{i,n}$ is the original signal value at time t_n.

1.2 FMRI data analysis

The fundamental division between the data analysis methods applied in this Thesis is their classification as model- or data-based approaches. The model-based analysis, in which temporal covariates are used to model the expected brain responses, represents the conventional way to determine brain activations from the fMRI data. Specifically, the user predicts the brain responses on the basis of the known stimulus timing but may also include other covariates into the model. The general lineal model is fitted to the data, and estimated parameters are then statistically tested. The final results are represented as statistical parametric maps.

In data-based methods, brain activity is determined from the data, without assumptions about the temporal behaviors of the signals. In data-based correlation analyses, signals from a certain brain area, or even from other subjects, can be used as a model to determine common activations within brain areas or between individuals.

ICA requires no *a priori* temporal information. Instead, it searches for spatially independent components, which add linearly. ICA, voxel-by-voxel and seed-point correlation analyses are the data-based methods discussed further below, after the basic preprocessing steps and GLM fitting of fMRI data are introduced.

1.2.1 Preprocessing of data

Movement or shape distortions in fMRI images can induce undesired variance in the functional image series, and thereby conceal the effects of interest or introduce false positive findings in statistical analysis. Voxel-based analysis methods assume that the voxel in a certain location represents the same part of the brain in a time series of successive functional images. The preprocessing of the fMRI data corrects for possible violations in spatial alignment with a set of spatial transformations. Preprocessing typically includes the realignment of the fMRI images, coregistration, normalization of images into a standard space (Friston et al., 1995; Ashburner and Friston, 1999), and spatial smoothing.

Realignment: Subject's head movement during fMRI scanning can lead to misalignments of successive functional images. Consequently, the same voxel in successive images of an imaging series may not represent the same brain area. The realignment procedure corrects for these misalignments by a six-parameter least-squares transformation (with three orthogonal directions and three rotations).

Coregistration: Individual functional and anatomical images are aligned by rigid-body transformations in the coregistration process. The mean functional image, for example, can serve as a reference image into which the anatomical image is coregistered.

Spatial normalization: The prerequisite for group analysis or inter-subject averaging of fMRI data is that the images are transformed into the same space. The Montreal Neurological Institute (MNI) provides one such standard brain space in terms of a template formed by 512 individual brains. Normalization algorithm (in SPM2) minimizes the sum of squared differences between the images that will be normalized and the template image (or a linear combination of several templates). The procedure starts with a 12-parameter affine transformation; first the whole head is matched, and then only the brains are co-registered by weighting the template voxels in a proper way. After initial transformations, nonlinear deformations are determined as a linear combination of low-frequency basis functions (three-dimensional discrete cosine transform set). The parameter estimates can be found within a

Bayesian framework, maximizing the posterior probabilities of deformation parameters for the given data.

Smoothing: Spatial smoothing further suppresses noise, as well as anatomical and functional differences between subjects thereby allowing better inter-subject averaging (Frackowiak et al., 2004). After smoothing, the errors are more normally distributed, which is required for inferences in statistical parametric tests. Typically, spatial smoothing is carried out by convolving functional images with a Gaussian kernel.

1.2.2 Statistical parametric mapping based on the general linear model

The conventional approach to analyze fMRI data is to model the time behavior of the measured brain responses and linearly fit the predicted model to the measured data. The general linear model is

$$\mathbf{x} = \mathbf{G}\boldsymbol{\beta} + \mathbf{e}, \mathbf{e} \sim N(0, \sigma^2\mathbf{I}), \tag{6}$$

where $\mathbf{x}$ is a column vector that contains the measured voxel signal (a time series of voxel values), $\mathbf{G}$ is the design matrix, where columns *g(t)* contain the temporal covariates to model the measured signal, and $\boldsymbol{\beta}$ are the parameters to be estimated. The error $\mathbf{e}$ is assumed to comprise independent and identically distributed normal variables with mean zero and variance σ^2; $\mathbf{I}$ denotes the identity matrix. The design matrix $\mathbf{G}$ can include both explanatory variables, *e.g.*, knowledge about the stimulation timing *s* convolved with the HRF *h*: $g(t) = \Sigma_{k=-\infty}^{\infty} h(k)s(t-k)$, and pre-known confounds, such as movement parameters. The estimated parameters $\hat{\boldsymbol{\beta}}$ are obtained as a maximum likelihood solution, which equals the ordinary least-squares solution under the above error assumptions

$$\hat{\boldsymbol{\beta}} = (\mathbf{G}^{\mathrm{T}}\mathbf{G})^{-1}\mathbf{G}^{\mathrm{T}}\mathbf{x}, \tag{7}$$

minimizing the squared error $\sum_{t=1}^{N} e_t^2$.

The BOLD signal contains considerable amounts of low-frequency noise, which can occur at the same frequencies as the hemodynamic effects of interest. These serial correlations with the fMRI data violate the assumptions of the GLM noise model (Zarahn et al., 1997), and they can be handled utilizing auto-regressive (AR) models (Bassett and Bullmore, 2006). Serial correlations and other filtering can be included in the GLM (6) by matrix multiplications, which lead to a generalized linear model. In practice, restricted-maximum-likelihood estimation is often used, since it allows the estimation of both model and autocorrelation parameters simultaneously (Friston et al., 2002).

After parameter estimation, the statistical significance of the estimates can be tested with *t*-statistics

$$t_{df} \sim \frac{\mathbf{c}^{\mathrm{T}}\hat{\boldsymbol{\beta}}}{\mathrm{STD}(\mathbf{c}^{\mathrm{T}}\hat{\boldsymbol{\beta}})}, \tag{8}$$

where t_{df} is the *t*-value from the Student's distribution with degrees of freedom *df*, **c** is contrast vector defining the effects of interest by weighting the parameter estimates in an appropriate way, and STD denotes standard deviation.

Results can be generalized to the population from which the subjects are drawn by testing the individual contrast images (defined by parameter estimates $\hat{\boldsymbol{\beta}}$ and their weights in **c**) in the second-level random-effects analysis. In this Thesis contrast images were subjected either to one- or two-sample, or paired *t*-test for group-level comparisons.

1.2.3 Data-driven correlation analyses

Seed-point correlations

A simple way to determine the functional connectivity of certain region of interest (ROI) with other brain areas is to extract the signal from the ROI and correlate it with the rest of the voxels within the volume.

This kind of "seed-point" correlations have been effective in revealing functional connectivities between motor regions (Biswal et al., 1995), language-related areas (Hampson et al., 2002), or within visual areas (Hampson et al., 2004), as well as during complex cognitive tasks (Goebel et al., 1998).

Seed-point approaches have been also applied in the analysis of resting-state networks, referring to the brain areas which are active during rest or in the absence of external stimulation (Lowe et al., 1998; Fox et al., 2005, 2006). Moreover, alterations in functional connectivities obtained with seed-point correlations have been considered as indications of diseases, such as Alzheimer's disease, multiple sclerosis, epilepsy, and schizophrenia (Rogers et al., 2007; Auer, 2008), and recently also of diabetic neuropathic pain (Cauda et al., 2009).

The drawback of seed-point analysis is that it requires strong *a priori* hypotheses regarding the selection of the seed. Often the resulting connectivity maps depend strongly on the selected seed (Ma et al., 2007), which can be alleviated, *e.g.*, by conjunctions of several seed-point correlation networks (Fox et al., 2005).

Voxel-by-voxel correlations

Another quite recent approach in fMRI data analysis is to correlate the signal from one voxel with the signal from a corresponding voxel of another image series (Hasson et al., 2004). Such voxel-by-voxel correlations can be used to reveal both intra-subject (two imaging runs of the same subject are correlated; Golland et al., 2007) and inter-subject similarity, with respect to the external stimulation.

In this Thesis, the capability of voxel-by-voxel correlations to reveal networks related to extrinsic and intrinsic processing (Golland et al., 2007) is utilized. Extrinsic refers here to a network which is activated due to external stimulation, contrary to brain circuitries related to intrinsic processing. This fundamental division of brain activity into extrinsic and intrinsic networks is also supported by the clustering of posterior cortex activity into two large systems (Golland et al., 2008).

1.2.4 Independent component analysis

Basic principles

ICA is a method to estimate the signal sources and their linear mixing from the measured data by assuming that source signals are statistically independent.

The linear ICA model is

$$\mathbf{x} = \mathbf{A}\mathbf{s}\,, \tag{9}$$

where **x** denotes the multivariate or measured data, **s** represents independent source signals, *i.e.*, independent components, and matrix **A** includes the coefficients of the linear mixing and is therefore called a mixing matrix.

ICA algorithms solve simultaneously both **A** and **s**. In practical calculations the inverse matrix $\mathbf{W} = \mathbf{A}^{-1}$ is estimated, and then, independent components are obtained by

$$\mathbf{s} = \mathbf{W}\mathbf{x}\,. \tag{10}$$

The measured signal **x** is a linear mixture of source signals from which ICA estimates the original sources by requiring statistical independence of the components (Hyvärinen and Oja, 2000). The underlying principle for ICA is the maximization of non-gaussianity of the linear combination $y = \mathbf{w}^T\mathbf{x}$, by finding a suitable vector **w** that is a row of **W**.

Examples of mathematical measures for non-gaussianity are kurtosis that is calculated from the fourth statistical moment, or negentropy. Negentropy is defined as $J(\mathbf{y}) = H(\mathbf{y}_{\text{gauss}}) - H(\mathbf{y})$, where **y** is a random vector, $\mathbf{y}_{\text{gauss}}$ is a Gaussian random variable with the same covariance matrix as **y**, and *H(***y***)* is the differential entropy. Entropy describes the information content of the variable; the more unstructured the variable is, the larger its entropy. Among all random variables of equal covariance matrix, Gaussian variables have the largest entropy. Therefore, negentropy always equals, or is greater than, zero. In practical calculations, approximations of negentropy are used.

Several ICA algorithms have been introduced to solve the ICA estimation problem. They all share two common properties: a measure of non-gaussianity and an optimization algorithm, which in this study was FastICA (Hyvärinen and Oja, 1997; Hyvärinen, 1999).

Before the ICA estimation, the data are preprocessed by mean removal and whitening. The components of whitened data are uncorrelated and their variances equal unity. Whitening can be done using the eigenvalue decomposition of the covariance matrix. Then, the linear whitening transformation is $\mathbf{V} = \mathbf{D}^{-1/2}\mathbf{E}^{\mathrm{T}}$, where $\mathbf{E}$ is the orthogonal matrix of eigenvectors and $\mathbf{D}$ the diagonal matrix of eigenvalues. For the mean-removed data $\mathbf{x}$, whitened data $\tilde{\mathbf{x}}$ are given by

$$\tilde{\mathbf{x}} = \mathbf{D}^{-1/2}\mathbf{E}^{\mathrm{T}}\mathbf{x} = \mathbf{D}^{-1/2}\mathbf{E}^{\mathrm{T}}\mathbf{A}\mathbf{s} = \tilde{\mathbf{A}}\mathbf{s}\,, \tag{11}$$

where $\tilde{\mathbf{A}}$ is the new mixing matrix. The whitening process results in an orthogonal mixing matrix, which reduces the number of parameters to be estimated.

The dimension of the original data m can be reduced in the whitening process by discarding the smallest eigenvalues and eigenvectors from the eigenvalue decomposition (Pearson, 1901; Hyvärinen and Oja, 2000). Then, data are projected from the m-dimensional data space onto an n-dimensional subspace $\tilde{\mathbf{x}} = \mathbf{V}_n\mathbf{x}$. Dimension reduction is typically a reasonable preprocessing step in ICA of fMRI data, since the amount of statistically independent signal sources (typically few tens) is often less than amount of measured volumes (typically few hundreds).

ICA and fMRI data

Spatial, rather than temporal, ICA is usually applied for fMRI data, which means that ICs comprise spatially independent, not systematically overlapping brain regions or networks. In spatial ICA model $\mathbf{X} = \mathbf{AS}$, one volume of fMRI data comprises one row in data matrix $\mathbf{X}$, and, correspondingly, one row of $\mathbf{S}$ is an independent component. Columns of the mixing matrix $\mathbf{A}$ represent the estimated time course for each spatial IC.

ICs, the statistically independent signal sources which are related to brain activation, can be either task-related or transiently task-related (the signal vanishes before the stimulation ends or changes over time during stimulus repetition). ICs can also represent physiology-, scanner- or motion-related signals or noise components (McKeown et al., 1998; Calhoun and Adali, 2006). McKeown and Sejnowski (1998) have shown that activity-dependent fMRI signals and noise typically have non-gaussian distributions, and thereby ICA suits well for fMRI data analysis.

Group ICA

Similarities across several subjects can be studied by group ICA methods. Group comparisons in ICA, however, are not as straightforward as in GLM analysis, where the same model is fitted to the data of every single subject, and contrast images of individual responses are then statistically tested at group level. In ICA, the signals of individual subjects can have different

time courses, and after the ICA estimation the individual components are neither sorted nor ordered, and thus cannot be straightforwardly subjected to group analysis.

At least three approaches for basic group-ICA analysis have been suggested. Calhoun et al. (2001a) proposed a method which is applied in this Thesis. In this method, data from each subject are concatenated into the same aggregate data set, assuming that the data from different individuals are statistically independent observations. Data reduction is performed in two or three steps, beginning with individual-level reduction and followed by reduction of the aggregate data set (Calhoun et al., 2001a)

$$\mathbf{X} = \mathbf{R}^{-1}\begin{bmatrix} \mathbf{F}_1^{-1}\mathbf{Y}_1 \\ \vdots \\ \mathbf{F}_N^{-1}\mathbf{Y}_N \end{bmatrix}, \tag{12}$$

where $\mathbf{R}^{-1}$ and $\mathbf{F}_i^{-1}$ are the reducing matrices from principal-component-analysis decomposition for the group and for the individual subject *i,* respectively. Also matrix $\mathbf{R}$ can be divided to $\mathbf{R}_i$ according to individuals. $\mathbf{Y}_i$ represent individual preprocessed data, one row of which is one volume of fMRI data. *N* is the total number of subjects.

The ICA model is then

$$\begin{bmatrix} \mathbf{R}_1 \\ \vdots \\ \mathbf{R}_N \end{bmatrix}\hat{\mathbf{A}}\hat{\mathbf{S}} = \begin{bmatrix} \mathbf{F}_1^{-1}\mathbf{Y}_1 \\ \vdots \\ \mathbf{F}_N^{-1}\mathbf{Y}_N \end{bmatrix}, \tag{13}$$

from which the ICA algorithm searches for activations common to the whole group, producing a single set of group ICs. Further, individual responses can be traced by back-reconstructing the group data into individual ICs $\hat{\mathbf{S}}_i = (\mathbf{R}_i\hat{\mathbf{A}})^{-1}\mathbf{F}_i^{-1}\mathbf{Y}_i$. Subject-wise concatenation of data requires good spatial normalization of individual images into the standard space.

Another option for group ICA is to concatenate the data row-wise $[\mathbf{x}_1, \mathbf{x}_2 \ldots, \mathbf{x}_N] = \mathbf{A}[\mathbf{s}_1, \mathbf{s}_2 \ldots, \mathbf{s}_N]$, in which case spatial normalization is not needed (Svensen et al., 2002). This approach estimates a common time course for all subjects, as well as individual spatial maps. However, subject-wise concatenation of data (Calhoun et al., 2001a) appears superior to this type of row-wise concatenation, especially when unique sources are present (Schmithorst and Holland, 2004).

Esposito et al. (2005) suggested a third group-ICA method, in which the ICs are first estimated separately for each subject and then the corresponding ICs across subjects are found by utilizing similarity measures and self-organizing clustering.

Component sorting

After the IC analysis is completed, the components do not appear in any specific order. In mathematical terms this means that inserting a permutation matrix and its inverse into the model does not change the estimated sources, but it can change their order (Hyvärinen and Oja, 2000).

In the earliest fMRI studies involving ICA, ICs were ranked by their contribution to the original data, *i.e.,* by the root mean square of data comprised by a certain component, or alternatively the root-mean-square error, when data were reconstructed without the contribution of certain component (McKeown et al., 1998).

Often the goal in the fMRI analysis is, however, to differentiate among the set of components those that arise from neuronal sources and are related to the presented task or stimuli from those that are artifact or noise. One classical method is to sort the components using temporal criteria, such as the known stimulus timing (McKeown et al., 1998; Calhoun et al., 2002; Kansaku et al., 2005; Moritz et al., 2005), or by utilizing the design matrix defined for GLM analysis (McKeown, 2000; Hu et al., 2005). Ranking that is based on IC power spectra can be used if the stimuli are presented with constant periodicity (Moritz et al., 2003).

Canonical-correlation analysis applied after ICA is an example of advanced extension of methods that utilize temporal criteria in identifying relevant ICs. This approach can take into account physical or other measures of the stimuli and use features to concatenate the ICs into groups of components that best describe the given set of stimulus features (Ylipaavalniemi et al., 2009).

Similar to sorting according to temporal criteria, correlations can be calculated on a spatial basis using, *e.g.*, brain-atlas images for component sorting (van de Ven et al., 2004; Calhoun et al., 2008). In this case, ICs are sorted by their spatial consistency with the given template. Earlier, Gu et al. (2001) proposed component ordering that accounts only for the spatial structure of the activation map, favoring components of large activation clusters and suppressing patterns related to motion artifacts.

Finally, it is also possible to use sorting approaches that do not require information about stimulus timing; such methods rely on component reproducibility, or on the characteristics of ICs themselves. Component reproducibility across several estimation runs can be used both for reliability analysis of the ICs and for ranking the components either on an algorithmic level (Himberg et al., 2004; Yang et al., 2008; Zeng et al., 2009) or on data level, by varying the input of the algorithm (Himberg et al., 2004; Zeng et al., 2009).

Intrinsic spatio-temporal properties, such as kurtosis, one-lag autocorrelation or degree of spatial clustering of the ICs, have also been utilized both for component ranking

(Formisano et al., 2002) and classification (De Martino et al., 2007). Utilizing these properties complemented with other measures, such as skewness, temporal entropy and spectral power at certain frequency bands, it is possible to construct a multidimensional IC fingerprint separately for each IC. The pattern of the fingerprint then indicates to which class (either BOLD signal or specific types of artifact) the IC most likely belongs. Thus, the classification based on IC fingerprints can effectively segregate the BOLD-related components from other types of signal sources (De Martino et al., 2007).

2 Aims of the study

The overall aim of this Thesis was to gradually move from conventional block fMRI designs to more naturalistic experimental setups. The emphasis was on the data analysis methods. The specific aims of the individual studies were

***i*)** to find out whether the reduction and correction of heart-cycle-related artifacts by means of cardiac-gated image acquisition would improve the detection of tactile responses in the secondary somatosensory cortex (SII), and in the thalamus (Study 1).

***ii*)** to compare data-driven (ICA) and hypothesis-based (GLM) data analysis methods during the presentation of a rather naturalistic stimulus sequence comprising free viewing, hearing, and feeling touch (Study 2).

***iii*)** to introduce a new method for sorting the stimulus-related ICs and to apply it in a study of sensorimotor processing of audio-visual speech (Study 3).

***iv*)** to analyze resting-state fMRI data of chronic pain patients and to compare the spatio-temporal properties of their affective pain matrix between patients and the healthy control subjects (Study 4).

3 Methods

3.1 Subjects

Altogether 42 subjects (31 males and 11 females) participated in the fMRI experiments; two of these subjects were scanned in more than one experiment. Most subjects were university students, except in Study 4, where chronic pain patients were recruited from the Pain Clinic of the Helsinki University Central Hospital. The Ethics Committee of the Helsinki and Uusimaa Hospital District had approved all experiments and each subject signed an informed consent prior the scanning. Table 1 lists the number of subjects and their mean ± STD of the age.

Table 1. The number (*N*) and age distribution (in years) of subjects in Studies 1–4.

Experiment	*N*	Mean ± STD age
Study 1	10	23.6 ± 3.5
Study 2	6	27.6 ± 2.9
Study 3	10	26.7 ± 4.3
Study 4	20	50.7 ± 8.9

3.2 FMRI measurements

The fMRI data were measured at the Advanced Magnetic Imaging Centre of Helsinki University of Technology (currently Aalto University School of Science and Technology) using Signa VH/I 3.0 T MRI scanner (GE Healthcare).

Functional images were collected with following parameters: TR = 3 s (Studies 1–3) or 4 s (Study 4), TE = 32 s, matrix = 64 × 64, voxel size = 3 × 3 × 3 mm^3 (Studies 1–3) or 3 × 3 × 4 mm^3 (Study 4) with no gap in-between the slices, FOV = 20 x 20 cm^2, flip angle $\alpha = 90^\circ$ (Studies 1–3) or 75º (Study 4). The number of slices was 15 in Study 1, 44 in Studies 2 and 3, and 33 in Study 4.

Structural images were obtained with a T_1-weighted 3-D spoiled gradient sequence using TR = 9 ms, TE = 1.9 ms, $\alpha = 15^\circ$, preparation time = 300 ms, number of excitations = 2, slice thickness 1.4 mm, and FOV 24–26 cm depending on the subject's head size.

Cardiac-triggered image acquisition

Cardiac pulsations were monitored with a pulse oximeter that was attached to the subjects' left index finger. Fifteen slices were collected, evenly-spaced in time within 3 successive R–R intervals, which led to an effective TR of 2.5–3.16 s. The TW was set to 20% of the cardiac cycle, and TD lasted for 300 ms to ensure that image collection did not start before the end of the systole. For signal-intensity correction, two additional image series were collected with TR_1 = 1.5 s and TR_2 = 10 s (see Equation 3).

3.3 Data analysis

Preprocessing

The standard tools of SPM2 software were used for preprocessing of the fMRI data: realignment, normalization into MNI space, and smoothing with a 6-mm (3-mm in Study 1) full-width-at-half-maximum Gaussian filter. The group-ICA approach requires especially accurate spatial normalization. Therefore, to achieve the best possible anatomical consistency across subjects, in Studies 2–4 the skulls were removed from the images prior to normalization.

GLM-based analysis (Studies 1–3)

GLM-based analysis was carried out with SPM2. Table 2 lists the regressors and statistical thresholds applied in the group-level analysis. Serial autocorrelations were handled with AR(1)-model in each design.

Table 2. Details of the temporal regressors included in the GLM, and the applied statistical threshold at group level (*p*-value from *t*-test, and the extent defined as the minimum number of statistically significant voxels in a cluster) in Studies 1–3.

Experiment	Regressors based on stimulation	Stat. threshold *p* / extent
Study 1	Tactile: lip, fingers and toes + 6 realignment parameters (tot. 3 + 6 nuisance covariates)	0.005 / 20
Study 2	Video: faces, hands, houses; audio: tone pips, instructions, history; tactile: fingers (tot. 7)	0.0005 / 20
Study 3	Normal speech loud, soft and mute; reversed speech loud, soft and mute; tone pips loud and soft (tot. 8)	0.001 / 10

ICA (Studies 2–4)

Common ICs for the whole group of subjects were estimated with the group-ICA approach (GIFT software, http://icatb.sourceforge.net) using the FastICA algorithm. Before the ICA, the number of components (76, 41, and 48 in Studies 2, 3, and 4, respectively) was estimated with a minimum-description length algorithm (Li et al., 2007), inbuilt in GIFT.

Component ordering

Only a subset of the estimated ICs was selected for closer examination. In Study 2, the properties of the task-related components, which temporally correlated most with the different stimulation categories, were studied. In addition, several ICs, whose activation patterns spatially resembled the so-called resting-state networks (Fox et al., 2005; Damoiseaux et al., 2006), were reported. *A priori* knowledge was also utilized in Study 4 by focusing on ICs that

covered the rather well-characterized affective pain matrix (Apkarian et al., 2005); the reference IC comprised the precuneus and early visual cortices.

In Study 3, a new approach was proposed and applied for sorting the ICs according to their stimulus-relatedness. This approach combines two data-driven methods, namely ISC and ICA. First, the brain areas, which were related to the external stimulation, were defined in terms of ISC (described in more detail below), and then ICs were sorted according their spatial overlap with the ISC map. The sorting parameter SP for the i^{th} IC is defined as

$$\mathrm{SP}_i = \lambda r(\mathrm{ISC}, \mathrm{IC}_i) + (1-\lambda)\frac{\sum_{x,y,z}(\mathrm{ISC})_{x,y,z}(\mathrm{IC}_i)_{x,y,z}}{\sum_{x,y,z}(\mathrm{ISC})_{x,y,z}}, \quad (14)$$

where $r(.)$ denotes the spatial Pearson's correlation coefficient between the thresholded ISC map and IC_i (first term), which is combined with relative amount of overlapping voxels (second term); λ is a weighting parameter.

Spatial overlap was determined from binarized images in which voxels exceeding the given statistical threshold were set to 1 and others to 0. SP thus takes into account both the similarity in activation distributions of ISC and IC as well as the extent of common activated areas. In Study 3, both terms were equally weighted ($\lambda = 0.5$) and 10 ICs with the highest SP values were selected for further analysis. The result of the spatial sorting was compared with sorting based on temporal similarity of IC time courses between subjects.

Inter-subject correlation (Study 3)

The inter-subject correlation map was determined by first calculating the pair-wise voxel-by-voxel correlation images ($N = 45$ from 10 subjects). The Fisher transformation was applied to convert the pair-wise correlation coefficients to the normally-distributed variables. Correlation maps were then subjected to group analysis to test, in each individual voxel, whether the correlations deviated statistically significantly from zero (one-sample *t*-test: false-discovery rate $p < 0.01$, extent of activation at least 10 voxels).

Prior to these calculations, the realignment parameters and the global mean (whole volume average) signal were fitted to the data of each individual using GLM, and then, their effect was removed from the gray-matter voxels. Gray matter voxels were obtained with Freesurfer (http://surfer.nmr.mgh.harvard.edu/) segmentation (Fischl et al., 2004).

Seed-point correlations (Study 4)

Six sub-areas from the affective pain matrix (right and left anterior insula, right medial insula, left posterior insula, anterior medial cingulate cortex, and posterior ACC), and one from the visual cortex, served as seed regions for scrutinization of functional connectivity of the affective pain matrix. Seeds were selected on the basis of ICA results; for example, the right-

anterior-insula (RAI) seed was defined on the basis of spatial group difference (two-sample *t*-test showed decreased anterior insular activity in the patients compared with control subjects; see Figure 10 in Section 4.4), or they were other local *t*-test maxima within the ICs tested at the group level.

The seeds were spheres of 6-mm radius and an average fMRI-signal (preprocessed individual data) from them was fitted to the rest of the brain voxels to obtain individual connectivity maps. Group analysis was performed separately for patients and control subjects (one-sample *t*-tests, $p < 0.0001$; extent of 20 voxels), and the groups were then compared (two-sample *t*-test, $p < 0.001$; extent of 20 voxels).

4 Experiments

4.1 Cardiac-cycle-synchronized image acquisition improves activation detection in SII and thalamus (Study 1)

Experimental setup

We collected two cardiac-triggered and two conventional image series (148 volumes in each including four dummy scans). In addition, two 12-volume image series were measured to obtain data for correcting the signal variations caused by variable TR in cardiac-triggered imaging.

Subjects received 4-Hz pneumatic tactile stimuli to the right side of their body; two distinct sites on their lower lip, second and third fingers, and second and third toes. Stimuli were delivered to each location in blocks, which lasted nine volumes and were followed by seven-volume rest periods.

Results

Figure 2 compares signal-corrected data obtained by cardiac-triggered image acquisition (left) with the result of conventional analysis (right). Cardiac triggering with the related analysis improved the detection of tactile activations in the thalamus and SII. At group level, only cardiac-triggered images revealed thalamic activations and bilateral SII activations (for finger stimulation). Moreover, at individual level, activations were seen in more subjects during cardiac triggering than conventional imaging; 5 *vs.* 2 individuals in thalamus, and 6 *vs.* 3 in the medial SII cortex.

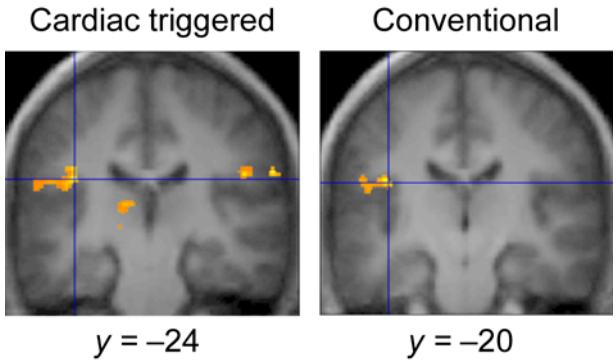

Figure 2. Brain activations in the SII and the thalamus related to tactile stimulation of right-hand fingers during cardiac-triggered image acquisition (left) and conventional imaging (right). One-sample *t*-test, thresholded with $p < 0.005$ and extent of activation ≥ 15 voxels. Modified from Study 1.

Both signal change and variance affect the statistical significance of the fMRI activations. Since signal change did not differ between conventional and cardiac-triggered image acquisitions, the improvement in activation detection was based on decreased variance due to the cardiac-triggering and post-acquisition signal correction.

Conclusion

Cardiac-triggered imaging can improve the detection of (touch-related) brain activations, both in the cortex and subcortical structures. The drawback of the method is, however, that fewer slices can be imaged within the same TR.

4.2 ICA is superior to GLM during complex stimulation (Study 2)

Experimental setup

Subjects followed a stimulation sequence, in which one of the unimodal auditory, visual, or tactile stimuli was always present, with no specific baseline or rest periods. Auditory stimulation consisted of either 0.1-s tone pips of different pitches, or continuous speech of a male reading either a story about the local university's history or guitar fingering instructions. Visual stimuli comprised silent videos which in different clips presented mainly faces, hands, or buildings in everyday environments. Pneumatic tactile pulses were delivered at 4 Hz to the second, third and fourth fingers of both hands. Each subject experienced the stimulation sequence twice during the 165-volume (8.25 min) functional imaging.

Results

ICA separated the sensory areas into spatially distinct networks according to the different sensory modalities or individual stimulus properties. Figure 3 shows an example of two ICs related to visual processing and two ICs related to auditory processing. The V1/V2 representation of lower visual field reacted to every type of visual stimuli. Signal in V5/MT responded similarly as V1/V2 to the videos containing faces and hands, but only weakly to the building videos, which contained less foveal movement. The lower panel in Figure 3 shows that the auditory cortex (ACx) reacts to every type of auditory stimulus, whereas superior temporal sulcus / middle temporal gyrus (STS/MTG) responds only to speech.

Altogether, brain areas that responded to visual stimuli, and were separated by ICA, comprised representations of the central upper and lower visual fields in V1/V2, of the peripheral visual field in V1/V2, posterior convexial cortex, V5/MT, and four other ICs near or within the parieto-occipital sulcus (POS).

Figure 4 compares the ICA and GLM-based analysis. The sub-areas of auditory and visual cortex activations revealed with GLM-based analysis were less extensive than those obtained by ICA. GLM-analysis also failed to show activations in the POS area and in the somatosensory cortices.

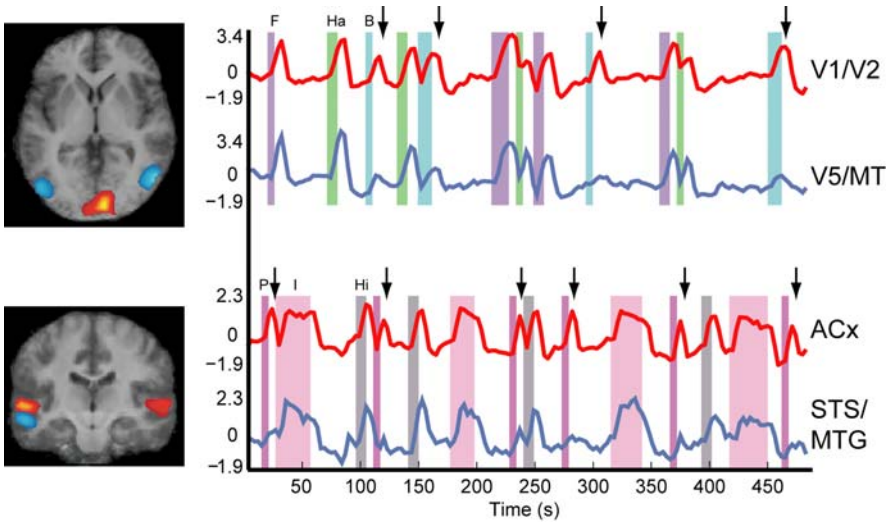

Figure 3. Average ICs and individual time courses from V1/V2 and V5/MT (red and blue ICs in the upper image) and from the auditory cortex (ACx) and the STS/MTG (red and blue ICs in the lower image). The arrows indicate differences in modality-specific responses, related either to visual or auditory processing (*z*-normalized values). Abbreviations: videos containing mainly F = faces, Ha = hands or B = buildings; auditory stimulus was either P = tone pips, I = guitar playing instructions, or Hi = local university history. Modified from Study 2.

Time courses in Figure **4** show that ICA-estimated BOLD responses (red) fit well to the predicted HRF model (black line) in early visual and auditory areas. In the primary somatosensory cortex (SI), however, the IC time course showed clear dependence on tactile stimulus presentation in the beginning of the stimulus series but it deviated from the predicted signal when the time between the stimulus blocks was shortest (6 s).

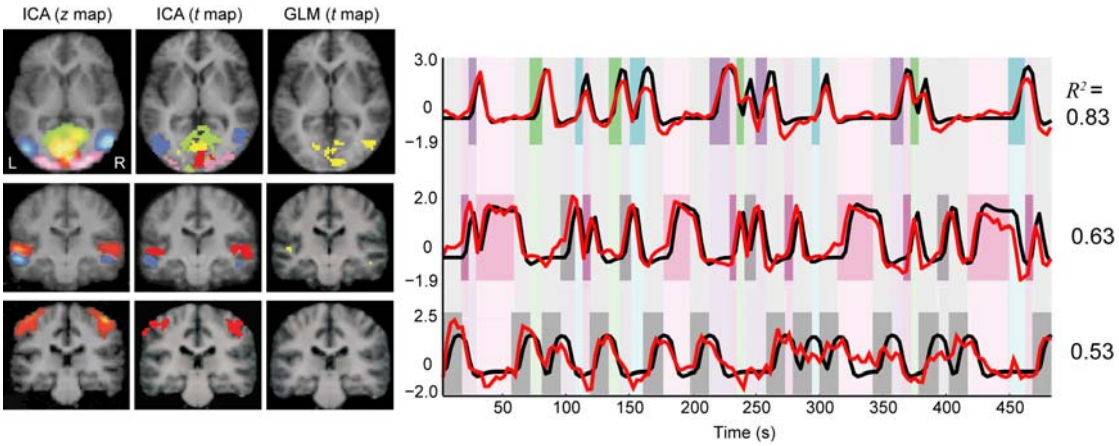

Figure 4. Comparison of ICA and GLM results. Black traces show the predicted hemodynamic models for visual, auditory, and tactile (from top to bottom) stimulation. The red time courses are the ICA estimates for the visual, auditory, and tactile components, respectively, related to the red ICs in spatial maps on the left. R^2 is the coefficient of determination between the HRF and IC time course. Colored areas behind the traces show when the certain unimodal stimulation was on; gray bars denote times of tactile stimulation, and other colors are the same as in Figure 3. Modified from Study 2.

Figure 5 illustrates that the time courses of stimulus-related ICs were very similar across subjects in early sensory areas and more variable in higher processing areas, except in SI, where individual signal variation was considerable already in the early processing areas.

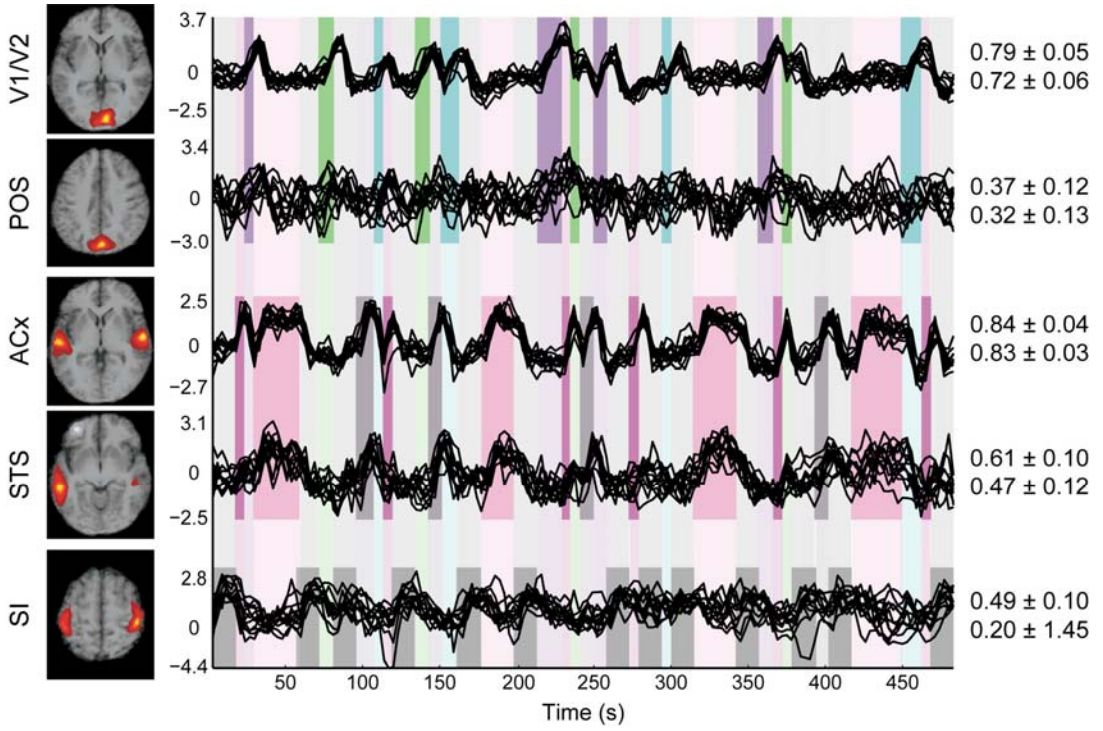

Figure 5. Individual signal variation in areas related to early sensory processing (V1/V2, ACx, and SI) and in areas related to higher-order processing (POS and STS/MTG). The mean ± STD inter-subject temporal correlation coefficients are given on the right; the upper values refer to the first and lower values to the second imaging session. Modified from Study 2.

Conclusion

Group ICA turned out to be a sensitive method to study brain responses elicited by complex naturalistic stimuli. It extracted functionally meaningful composites of activated brain areas even though only six subjects were studied, thereby showing superior performance compared with the GLM-based analysis. Results also indicated increased individual variability of the hemodynamic response in higher processing areas compared with early sensory cortices.

4.3 ISC–ICA sorts ICs related to audiovisual speech (Study 3)

Experimental setup

The loudness of continuous (8.5-min) audiovisual stimulation was varied between clearly-audible (loud), just audible (soft), and silent. Twice during the experiment, the stimulation was reversed in time or interrupted with tone pips, both having similar variation in stimulus as normal speech. Ten subjects were scanned twice during the experiment and 170 volumes were included in the analysis from both runs.

Results

Figure 6 presents the inter-subject correlation map, which was used in the IC ordering. Statistically significant similarity across subjects was evident in the temporal, occipital, and parietal areas, as well as in frontal areas (including Brodmann area 10).

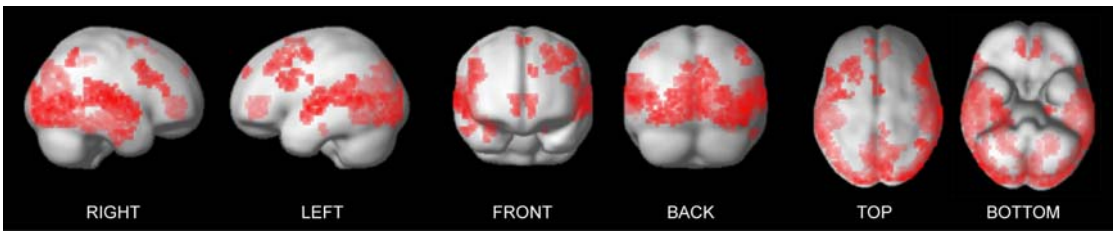

Figure 6. ISC map obtained by stimulation containing audiovisual speech, reversed speech, and tone pips. Modified from Study 3.

Combined ISC–ICA analysis revealed the most stimulus-related ICs. Among them were both sensory-processing areas and default-mode components, whose activity was modified similarly across subjects due to the external stimuli. Sorting based on the ISC map provided a physiologically reasonable order at least for the first ten ICs. Figure 7a shows the six most stimulus-related components based on ISC-map sorting. The first IC covers the auditory cortex in both hemispheres, the next four ICs cover different parts of visual cortices, IC6 agrees with the sensorimotor network of normal speech processing (described in more detail below), and IC7 is the default-mode component modified by the stimulation.

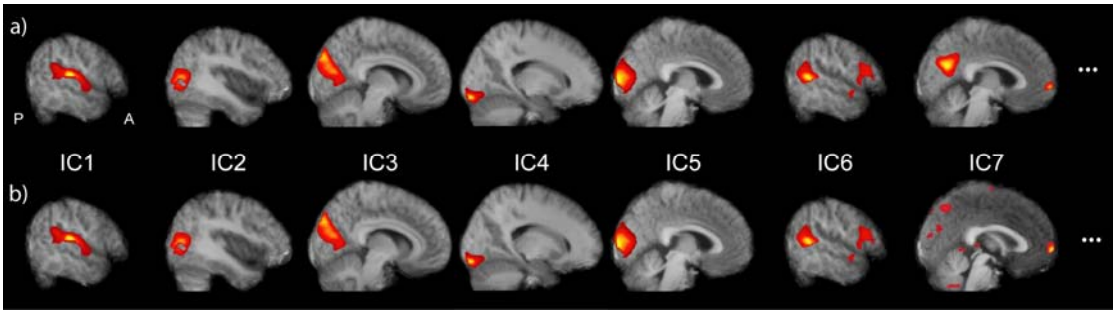

Figure 7. ICs sorted according to a) ISC-map and b) inter-subject temporal correlations (own unpublished result).

A comparable method to sort the ICs is to look for maximum correlations of IC time courses across subjects. Figure 7b presents the component order according to the statistically most significant temporal correlations. Up to the first six components, the order is the same as in the ISC-based sorting, whereas the spatial pattern of the seventh IC does not look physiologically meaningful.

In addition to activations in the auditory and visual cortices, ISC–ICA picked up a left-lateralized sensorimotor network (IC6) comprising the left STS, left anterior superior

temporal gyrus, left inferior frontal gyrus (IFG, including Broca's area), left premotor cortex (BA6), and the right inferior parietal lobule (IPL). IC6 reacted for normal speech, occasionally even more strongly for soft than loud speech. Contrary to the left-lateralized sensorimotor network, the right-lateralized MTG–IFG–IPL circuitry was activated more strongly for reverse than normal speech. This network showed transiently increased activity during every block, possibly related to the update of the content of the auditory working memory.

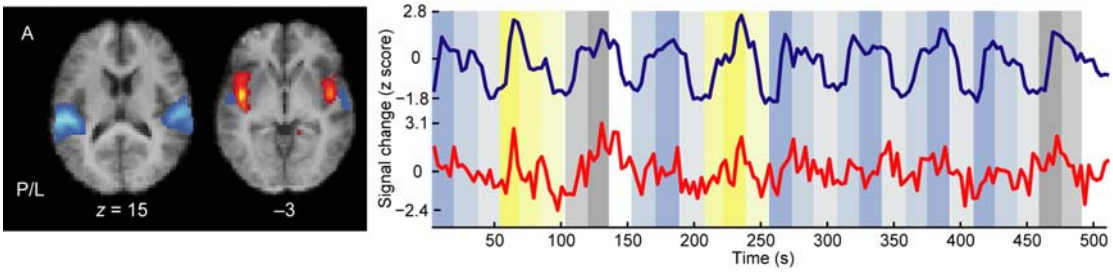

Figure 8. Left: ICs from auditory cortex (blue) and insula (red). Right: time courses for auditory cortex (blue) and insula (red) related to ICs presented on the left. Colors on the background show stimulation duration and type: shades of blue = normal speech, yellow = time reversed speech and gray = tone pips. The darker the color, the louder the stimulus. Modified from Study 3 (data from insula are own unpublished results).

Among the 10 most task-related components was also an IC, presented in red in Figure 8, that covered the insula in both hemispheres and showed, in general, rather similar task-dependence as the auditory cortex component (blue), but containing more high-frequency variation.

Conclusion

ISC maps first identified brain areas that were most strictly related to external stimuli. ICs, which were sorted by their spatial overlap with the ISC map, revealed detailed spatio-temporal properties of the independent sub-networks related to processing of audiovisual speech. Most importantly, the ISC analysis revealed the involvement of left-lateralized sensorimotor network during comprehension of speech of diminished intelligibility. The ISC–ICA approach therefore seems valid for various fMRI experiments applying naturalistic and continuous stimuli.

4.4 Spatio-temporal properties of resting-state networks are altered in chronic pain (Study 4)

Experimental setup

Resting-state brain activity was measured during four ten-minute fMRI scanning runs in chronic pain patients and in sex- and age-matched healthy control subjects. For a later control

analysis, heart and respiration rates of two patients and two control subjects were correlated with fMRI signals from selected seed areas.

Results

Two ICs belonging to the affective pain matrix—the bilateral lower insular cortices and the anterior cingulate cortex (ACC)—were selected for closer examination.

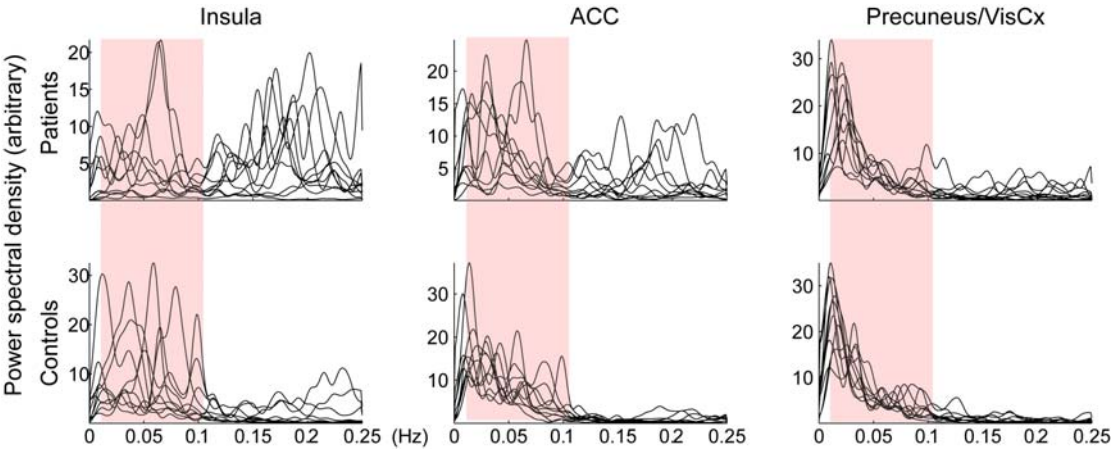

Figure 9. Individual power spectral densities in patient and control groups (upper and lower panels, respectively). The red area shows the frequency range typically examined in resting-state fMRI analysis. Modified from Study 4.

Figure 9 illustrates the power spectral densities of both groups. ICs covering the lower insula and ACC showed stronger spectral power at 0.12–0.25 Hz in patients than in control subjects; the difference was largest at 0.16 Hz. Precuneus/VisCx, used as a control site, did not show such an effect.

Figure 10 (left) shows that the right anterior insula (RAI) activation was suppressed in patients compared with healthy control subjects. Figure 10 (right) presents an example of statistically significant differences in functional connectivity between the groups, when posterior ACC served as a seed. In the control group, the anterior insula, posterior insula, and ACC were functionally connected, whereas in the pain patients, insula and ACC connections were disturbed.

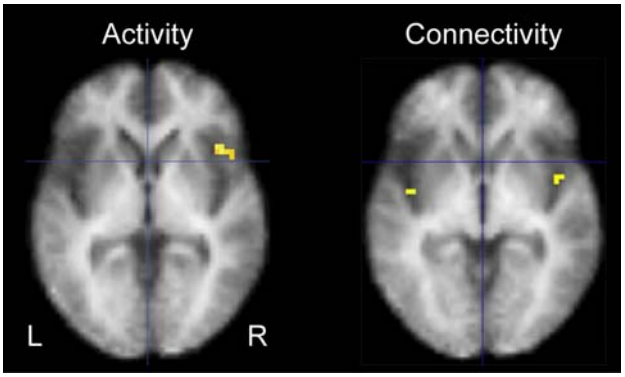

Figure 10. Statistically significant differences (control subjects *vs.* patients) both in activity (left) observed by comparing individual ICs comprising bilateral insula (own unpublished result), and in connectivity (right) for ACC as the seed-area (two-sample *t*-test; $p < 0.001$, extent 10 voxels at MNI *z*-coordinate 0).

In the control analysis with 4 subjects, fMRI signals did not correlate with respiration rate and correlated only weakly (~0.1) with the R–R interval time series. Neither measurement revealed differences between the two pain patients and two control subjects.

Conclusion

Spatio-temporal properties of resting-state activity were altered in patients suffering from chronic pain compared with healthy control subjects. Since heart-rate correlations with fMRI signals were small in all seed areas, the cardiac pulsations can be considered unlikely causes for the patients' faster fluctuations. The exact reason for aberrant temporal behavior in the patient group thus remains unknown, but it could be related to altered autonomic nervous system (ANS) activity.

The altered spectral content between the groups was observed since we did not apply conventional low-pass filtering of resting-state data with cut-off around 0.1 Hz. The results suggest that opening the frequency band beyond the conventional filtering may be occasionally beneficial in revealing differences in some patient groups where the neural and/or hemodynamic activity is altered. To better understand the mechanisms of accentuated fluctuations and their relation to altered functional connectivity, the ANS activity during fMRI (resting-state) experiments should also be monitored.

5 General discussion

The fMRI studies of this Thesis evolved gradually from discrete on–off stimulus presentation to more continuous and complex stimulation. Comparison between the ICA and ISC data-based techniques with the model-based GLM approach was possible in studies containing stimulus blocks, even though the complexity (from unimodal to multimodal) and continuity (from block presentation to continuous stimulation) were increased. Although previous comparisons of the methods have yielded comparable results, or favored the sensitivity of GLM-based approach (Calhoun et al., 2001b, 2001a), the results obtained in this Thesis indicated that during naturalistic stimulation data-driven methods can offer more extensive and detailed information about brain activations than do temporal covariates in GLM-based analysis. In future fMRI experiments, the methods studied in this Thesis can fairly reliably be applied to truly continuous stimulus conditions, in which it is difficult, if not impossible to use stimulus-related temporal covariates as will be discussed below.

5.1 Assumptions and outcomes of the analysis methods

Human brain is active all the time. Fluctuations of brain's signaling and hemodynamic activity occur even in the absence of any sensory stimulation, as has been shown by studies of resting-state or default-mode activity (Fox and Raichle, 2007). Even during rest, the brain is organized into functionally connected networks, whose activity and connectivity may be altered by stimulation or cognitive demands (Gusnard et al., 2001; Greicius et al., 2003; Fransson, 2006; Hasson et al., 2009a). By means of fMRI, it is possible to probe these resting-state fluctuations and functional organization of the human brain, as was done in Study 4 of this Thesis. Typically, stimulus-induced brain activations have been examined by presenting discrete sensory stimuli to subjects and thereafter analyzing responses time-locked to the stimuli. However, when continuous stimulation is presented with no rest periods in between, it is more complicated to find out which of the observed fluctuations are related to the external stimuli or tasks and which just reflect intrinsic or resting-state activity.

What is task-related?

Definition of *task-relatedness* is an obvious matter of consideration when naturalistic stimuli lead to increasingly complex behavior of the hemodynamic signal. In GLM analysis, task relatedness is an inbuilt property and the basic assumption of the analysis method itself. The applied temporal covariates or models precisely define which phenomena (either brain response or confound) are assumed to occur at certain time instances and thereby be detectable in statistical testing. The temporal covariates are typically convolved with the HRF,

which often serves as a proper model for BOLD impulse response, but which also may vary depending on the subject, brain area or be modified by disease.

Most likely, the best signal fits with the HRF-convolved covariates are obtained in the visual cortices, from which the HRF model has originally been estimated (Boynton et al., 1996) and similar HRF characteristics have also been found in the early auditory-processing areas (Josephs et al., 1997). However, HRF may depend on brain area and the stimulus. For example ICA has revealed that even simplistic flickering checkerboard stimuli can induce variable hemodynamic responses in primary visual areas (Duann et al., 2002). In this Thesis, Study 2 showed that a striking deviance from the expected BOLD behavior in the primary somatosensory projection areas: the SI response deviated significantly from the predicted model for short inter-block intervals and was the likely reason for the invisibility of SI activation in the conventional GLM-based analysis.

If the research question focuses only on a certain restricted brain area, instead of the whole brain volume, it would be reasonable to estimate the shape of the HRF for that particular region. Both the estimation efficiency and the detection power cannot, however, be maximized simultaneously. In naturalistic stimulus settings, in which large networks consisting of nodes in several brain areas can be simultaneously active, the estimation of the HRF shape may thus not be reasonable.

To avoid the difficulty of defining a temporal model for brain responses, the brain activity of one individual can be predicted with the data from another person who was subjected to the same stimulation. This approach was taken in the ISC analysis, in which the task-relatedness was defined as similarly modulated brain responses across subjects in terms of statistically significant correlations.

Whereas both GLM and ISC rely on temporal models—GLM in a user- and ISC in a data-driven manner—ICA does not require any information about temporal behavior of the signals. The underlying assumption of ICA in fMRI analysis is the spatial independence of estimated components and, therefore, ICA provides information about the signal's temporal behavior beyond any predefined temporal models. ICA, as such, does not identify which of the estimated ICs are task-related and this information needs, therefore, to be achieved by other means as discussed in more detail below.

Properties of the ISC map

Correlations of brain responses of one individual with the responses of another individual have revealed that large brain areas can be activated in unison between different people (Hasson et al., 2004). In Study 2, the hemodynamic signals were relatively similar in the early projection areas but the signals became more variable in areas related to higher-order processing. Despite this variability, the ISC map in Study 3 demonstrated activations beyond

the early sensory areas. The ISC map included brain areas related to cognitive processes, such as the frontal cortex, and brain areas of the default-mode network. These findings imply that the activations even in non-sensory brain areas can be modulated by external stimuli rather similarly across individuals. These observations are in line with the first ISC studies: During free viewing, inter-subject synchronization was especially strong in early sensory cortices, but significant similarity occurred also in association cortices (Hasson et al., 2004).

Recently, voxel-by-voxel correlation analysis has been applied for the study of the hierarchy of time scales of cortical processing during free viewing (Hasson et al., 2008). In autistic subjects, ISC showed diminished similarity between individuals and intra-subject correlations further demonstrated idiosyncratic activation patterns (Hasson et al., 2009b). Although both of these examples convincingly show that voxel-by-voxel correlations provide an effective analysis tool as such, in this Thesis ISC was primarily used to facilitate the selection of stimulus-related components in ICA.

ISC map in the selection of stimulus-related ICs

Temporal criteria have dominated the segregation of stimulus-related ICs (see *Component sorting* in section 1.2.4): either temporal covariates similar to those in GLM or other stimulus-related features have been correlated with IC time courses. In Study 2, ICs were selected on the basis of *a priori* information of activated brain areas and according to their temporal dependence on the external stimulation. Study 3 provided a slightly more sophisticated approach: ICs were sorted with the help of the ISC map. Since ISC illustrates brain areas related to processing of external stimuli in the form of a spatial map, no temporal models of signal behavior were needed after ICA.

One difficulty in ISC-map-based IC sorting is that the user needs to determine how many of the ordered components are truly stimulus-related and of interest. In fact, we could have used the ISC map to constrain the estimation of the ICs into active voxels of the map. Then, only areas that are known to be modified by the external stimulation would have been included and sub-partitioned in ICA, and consequently, all ICs could have been considered to be stimulus-related. This approach, however, may not be the most desirable, since ICs obtained with the statistical independence criterion can also unravel connections among brain areas that are not strongly temporally correlated between subjects and, thus, would remain invisible in the ISC map.

In Study 4, (seed-point based) correlation analysis yielded comparable, but still distinct results compared with ICA, which separated the areas of interest—insula and ACC—into two different components. The applied group analysis, based on individual ICs, revealed weakened activity in the patients' RAI, and seed-point correlations further confirmed that the connections within the affective pain matrix were disturbed in the patient group. Correlations,

which measure dependence between random variables using second-order statistical moments most often provide distinct, but complementary, information about functional connectivity or stimulus-related brain networks compared with ICA that is based on higher-order statistics. Therefore, the ISC map is most likely best applied when it facilitates, rather than defines or constricts, the selection of stimulus-related ICs.

A method related to ISC mapping involves determining the most similar IC time courses between individuals (Bartels and Zeki, 2004). Among the most significant ICs in Study 3, the temporal-correlation approach revealed the first six components in a similar order, but the following components were spatially more unlikely candidates for the most stimulus-related ICs. Importantly, the default-mode component did not survive IC-time-course correlations, although it was clearly visible in voxel-by-voxel correlations in the ISC map. Thus, among the existing methods, ISC–ICA has two advantages: (*i*) ranking the components according to their stimulus-relatedness does not impose prerequisites for the stimulation or task, or their timing, and (*ii*) revealing even sensitivity of default-mode or intrinsic networks to external stimulation.

In future fMRI studies, ISC-based IC sorting combined with finger-print (see Section 1.2.4) classification and selection of BOLD-related ICs (in contrast to noise or artifacts) could possibly provide more detailed insights for the selection of stimulus-related ICs. This could confirm that sorted components are related to BOLD signal changes, or alternatively, only ICs related to BOLD signal changes could be sorted.

5.2 Individual signal variations and group inferences

In Studies 2 and 4, we made observations on the individual IC time courses. Study 2 showed that stimulus-related signals are very similar in early visual and auditory processing areas and become more variable in brain areas related to higher processing. In Study 4, the individual time courses indicated differences in temporal dynamics between pain patients and healthy control subjects, and these differences were also confirmed with statistical testing. This type of closer scrutinization of individual time courses is still rather rare in fMRI studies that typically visualize results as statistical maps depicting spatial distribution of statistically significantly activated brain areas.

In group ICA that applies subject-wise concatenation of the data, the individual ICs and corresponding time courses are obtained by back-projecting data from aggregate components into single-subject level. Although individual subjects are initially considered as statistically independent observations, the resulting back-projected ICs can be tuned and constrained by the initial aggregate ICs. However, this procedure did not seem to have any major effect, because the individual IC time courses reported in this Thesis strongly resembled the true signal behavior within the brain areas covered by the spatial component.

In Studies 2 and 3, we compared the group-level inferences obtained with GLM and ICA. Both studies indicated that in almost continuous stimulus presentations, ICA can provide more detailed information about brain processes related to the stimulation. In group ICA, however, one or several individual back-projected ICs are known to carry information from the aggregate components, whereas in GLM-based group analysis, such *a priori* information does not exist. These conceptual differences between group-inference testing in ICA and GLM may have an effect on the conclusions made of the sensitivities of the methods to detect brain activations. How severe these possible confounds are in practice remains to be studied.

Langers (2009) recently proposed an alternative framework for ICA group-level testing to overcome these limitations: individual ICs are matched with aggregate components and selection bias is also accounted for.

5.3 FMRI activity in the presence of physiological pulsations

Besides reflecting neuronal activity, the fMRI signal includes, or can be disturbed by, several non-neuronal factors, such as other physiological signals, scanner-related artifacts and other types of noise. This Thesis paid attention to the elimination of physiological noise from fMRI signal, specifically noise related to cardiovascular pulsations and its possible contamination of ICs.

Elimination of cardiac pulsations by cardiac-triggered imaging

In Study 1, the effects of cardiac pulsations were successfully eliminated both from the deep brain areas and the cortex by synchronizing the image acquisition with cardiac function. This method, despite its benefits, is rather time-inefficient since it would have been possible to collect 2.4–3 times more volumes within the same total imaging time by using conventional image acquisition without cardiac triggering. The increased number of time points would have improved the statistical inference, theoretically approximately 1.6–1.7-fold, which could compensate for the inferior performance of conventional imaging compared with cardiac triggering. Moreover, the constant TR of 3 s would have enabled whole-brain coverage in the functional images, whereas with cardiac triggering, only a third of the slices could be collected within one volume, leading to severely limited spatial coverage.

For these reasons, cardiac-triggered image acquisition should be applied only after careful consideration. Results shown here are in line with the common understanding that cardiac-triggered fMRI is most useful for analysis of signals originating from deep brain areas, where the pulsations are strong and the smaller spatial coverage of functional images is not a problem.

FMRI signals carry information of several signal sources

Study 1 further implied that the effect of pulsations can be significant even in the cortex, especially in the proximity of big vessels. Both the second somatosensory cortex SII, examined in Study 1, and the insula reported in Studies 2–4, lie close to vessels of the internal carotid artery. The obvious need to control for the contribution of cardiac pulsations in the fMRI signal was therefore revisited in Study 4, in which the connection between higher insular frequencies and heart rate was studied in post-hoc analyses. The weak (~0.1) positive correlation between the hemodynamic variability and heart rate explains only a minor part of the signals and does not give support for pulsation-related difference between the groups; however, these analyses were carried out only in two patients and two control subjects.

In Study 2, the IC covering the insula was classified as one of the components related to intrinsic processing, but in Study 3, the insular IC turned out to be stimulus-related. Also, the temporal behavior of the insular IC supported this classification in Study 3: the activity followed stimulus presentation in a similar manner as in the auditory cortex, but the insula contained more spectral power at higher frequencies. Along similar lines, in Study 4, the insular IC contained more power in higher frequencies than the other ICs. In chronic pain patients, RAI activity appeared diminished compared with healthy control subjects; the reason could be related to changes in the pain patients' interoceptive processing (that is of stimuli, which originate inside of the body; Craig, 2009) in pain patients.

Study 4 (showing negligible signal correlation with the ECG signal and with no difference between patients and control subjects) supports the view that insular fMRI activity recorded in this study most likely reflects neuronal activation. One possible, albeit unconfirmed, suggestion would be that the insular neuronal signals are modulated by ANS function. Another option is that the insular fMRI signals have contributions both from neuronal processes and from physiological pulsations. If these sources add nonlinearly, they may not be separated by linear methods such as ICA.

Issues of temporal filtering of fMRI data

From the methodological viewpoint, Study 4 has two implications for future fMRI studies. The first is the necessity to monitor ANS function (Gray et al., 2009), either to reveal possible correlates between ANS function and fMRI signal, or to exclude those signal sources which could hypothetically affect the signal behavior, but in reality do not.

The second implication is that the conventional filtering of fMRI data may in some cases be too conservative. Resting-state fMRI studies typically focus on frequencies below 0.08–0.1 Hz, where most of the BOLD-signal power is concentrated, whereas heart rate effects and respiratory fluctuation are typically seen at 0.6–1.2 Hz and 0.1–0.5 Hz,

respectively (Cordes et al., 2001). These potential artifacts should of course be avoided as much as possible, but too strict filtering may hinder the visibility of altered brain activity, especially changes in hemodynamic behavior in some pathological conditions. The biggest difference between healthy control subjects and pain patients occurred around 0.16 Hz. Hence, in certain cases, a more appropriate limit for low-pass filtering would be above this value. These low-frequency BOLD signal oscillations are still within the 0.16 Hz limit below which, according to Logothetis (2003), neuronal responses can be estimated.

5.4 Future perspectives

Future neuroimaging studies will increasingly exploit continuous and complex stimulus conditions to study human brain function in naturalistic settings. Neurocinematics (Hasson et al., 2008), for example, has already established a firm ground for utilizing cinema as a controllable presentation of naturalistic environments to study, *e.g.*, inter-individual similarity. Studies in social neuroscience will increasingly concentrate on on-line communication between individuals, and the long-term aim in these studies is understanding the neural basis of social interaction involving at least two people (Hari and Kujala, 2009). Common to these studies is that they mimic continuous real-life-like situations and phenomena which evolve only during long periods of time and cannot be effectively characterized with static stimuli presented discretely in time.

Necessity of additional measures

Increasing stimulus complexity and continuity can consequently mean less controllability of stimulation sequences compared with traditional simplistic stimulation. To compensate for this, additional measures may be needed. One possibility, with increasing popularity, is to follow the subject's gaze during the experiment with an MR-compatible eye-tracking camera. Eye-gaze monitoring can reliably reveal which features the subject really looks at during the continuous stimulus flow, and consequently, most likely pays attention to. Another potentially useful measure obtainable with the eye-tracking camera is the pupil diameter (Critchley et al., 2005), which can serve as an indicator of arousal or other ANS-mediated mechanisms. More generally, as mentioned in the previous chapter, monitoring ANS function, such as heart rate (Critchley et al., 2003; Yang et al., 2007; Napadow et al., 2008), respiration or electrodermal activity (Critchley et al., 2002), will be of increasing importance in future fMRI experiments assessing either external stimulus-related processes or intrinsic brain function. What is more, the advantages of additional monitoring may not be constrained to control purposes only, but most likely would be beneficial for fMRI data analysis: the more complementary data are available for analysis purposes, the more profound and detailed becomes the understanding of the underlying phenomena.

New ways to analyze fMRI data

In this Thesis, data-based methods, ICA and ISC, were considered to be especially useful in the analysis of naturalistic stimulus conditions. However, other new ways to analyze fMRI data have been introduced, such as multi-voxel-pattern analysis techniques (Haynes and Rees, 2005; Kamitani and Tong, 2005; Norman et al., 2006) and analysis of cortical hubs (Bassett and Bullmore, 2006; Buckner et al., 2009).

Multi-voxel-pattern analysis reveals fMRI activation patterns that represent certain stimuli or mental states. Trained classifiers can then search for or "decode" these patterns from novel and untrained data sets. Recent remarkable advances in utilizing multi-voxel-pattern analysis include, *e.g.,* decoding of the speaker identity and the speech content (Formisano et al., 2008), or recognition of the novel scene images viewed by the subject (Kay et al., 2008).

Hub analysis reveals connectedness of brain networks. The advantage of the method is that, similar to ICA, no user-defined seed regions are needed for determining the connectivity. We have obtained promising preliminary hub analyses that complement the results of Study 4 on the reduced functional connectivity of insulae in chronic pain patients (Ramkumar et al., 2010).

Studies on human brain activity during naturalistic stimulation are still in their infancy. In this Thesis, the stimulation became gradually more continuous and complex, which allowed controllability with conventional analysis methods. The results and observations seem potentially useful for future fMRI research of naturalistic stimuli, either as such, or in combination with other more advanced analysis methods.

Bibliography

Apkarian AV, Bushnell MC, Treede RD, Zubieta JK (2005). Human brain mechanisms of pain perception and regulation in health and disease. Eur J Pain 9:463–484.

Ashburner J, Friston KJ (1999). Nonlinear spatial normalization using basis functions. Hum Brain Mapp 7:254–266.

Auer DP (2008). Spontaneous low-frequency blood oxygenation level-dependent fluctuations and functional connectivity analysis of the 'resting' brain. Magn Reson Imaging 26:1055–1064.

Bandettini PA, Wong EC, Hinks RS, Tikofsky RS, Hyde JS (1992). Time course EPI of human brain function during task activation. Magn Reson Med 25:390–397.

Bartels A, Zeki S (2004). The chronoarchitecture of the human brain–natural viewing conditions reveal a time-based anatomy of the brain. NeuroImage 22:419–433.

Bassett DS, Bullmore E (2006). Small-world brain networks. Neuroscientist 12:512–523.

Belliveau JW, Kennedy DN, Jr., McKinstry RC, Buchbinder BR, Weisskoff RM, Cohen MS, Vevea JM, Brady TJ, Rosen BR (1991). Functional mapping of the human visual cortex by magnetic resonance imaging. Science 254:716–719.

Belliveau JW, Rosen BR, Kantor HL, Rzedzian RR, Kennedy DN, McKinstry RC, Vevea JM, Cohen MS, Pykett IL, Brady TJ (1990). Functional cerebral imaging by susceptibility-contrast NMR. Magn Reson Med 14:538–546.

Biswal B, DeYoe AE, Hyde JS (1996). Reduction of physiological fluctuations in fMRI using digital filters. Magn Reson Med 35:107–113.

Biswal B, Yetkin FZ, Haughton VM, Hyde JS (1995). Functional connectivity in the motor cortex of resting human brain using echo-planar MRI. Magn Reson Med 34:537–541.

Bloch F, Hansen WW, Packard M (1946). Nuclear induction. Phys Rev 69:127.

Boynton GM, Engel SA, Glover GH, Heeger DJ (1996). Linear systems analysis of functional magnetic resonance imaging in human V1. J Neurosci 16:4207–4221.

Buckner RL, Sepulcre J, Talukdar T, Krienen FM, Liu H, Hedden T, Andrews-Hanna JR, Sperling RA, Johnson KA (2009). Cortical hubs revealed by intrinsic functional connectivity: mapping, assessment of stability, and relation to Alzheimer's disease. J Neurosci 29:1860–1873.

Buxton RB. 2009. Introduction to functional magnetic resonance imaging. 2 Edition: Cambridge University Press.

Calhoun VD, Adali T (2006). Unmixing fMRI with independent component analysis. IEEE Eng Med Biol Mag 25:79–90.

Calhoun VD, Adali T, Pearlson GD, Pekar JJ (2001a). A method for making group inferences from functional MRI data using independent component analysis. Hum Brain Mapp 14:140–151.

Calhoun VD, Maciejewski PK, Pearlson GD, Kiehl KA (2008). Temporal lobe and "default" hemodynamic brain modes discriminate between schizophrenia and bipolar disorder. Hum Brain Mapp 29:1265–1275.

Calhoun VD, Adali T, McGinty VB, Pekar JJ, Watson TD, Pearlson GD (2001b). fMRI activation in a visual-perception task: network of areas detected using the general linear model and independent components analysis. NeuroImage 14:1080–1088.

Calhoun VD, Pekar JJ, McGinty VB, Adali T, Watson TD, Pearlson GD (2002). Different activation dynamics in multiple neural systems during simulated driving. Hum Brain Mapp 16:158–167.

Cauda F, Sacco K, D'Agata F, Duca S, Cocito D, Geminiani G, Migliorati F, Isoardo G (2009). Low-frequency BOLD fluctuations demonstrate altered thalamocortical connectivity in diabetic neuropathic pain. BMC Neurosci 10:138.

Chuang KH, Chen JH (2001). IMPACT: image-based physiological artifacts estimation and correction technique for functional MRI. Magn Reson Med 46:344–353.

Cordes D, Haughton VM, Arfanakis K, Carew JD, Turski PA, Moritz CH, Quigley MA, Meyerand ME (2001). Frequencies contributing to functional connectivity in the cerebral cortex in "resting-state" data. AJNR Am J Neuroradiol 22:1326–1333.

Craig AD (2009). How do you feel–now? The anterior insula and human awareness. Nat Rev Neurosci 10:59–70.

Critchley HD, Melmed RN, Featherstone E, Mathias CJ, Dolan RJ (2002). Volitional control of autonomic arousal: a functional magnetic resonance study. NeuroImage 16:909–919.

Critchley HD, Tang J, Glaser D, Butterworth B, Dolan RJ (2005). Anterior cingulate activity during error and autonomic response. NeuroImage 27:885–895.

Critchley HD, Mathias CJ, Josephs O, O'Doherty J, Zanini S, Dewar BK, Cipolotti L, Shallice T, Dolan RJ (2003). Human cingulate cortex and autonomic control: converging neuroimaging and clinical evidence. Brain 126:2139–2152.

Damadian R (1971). Tumor detection by nuclear magnetic resonance. Science 171:1151–1153.

Damoiseaux JS, Rombouts SA, Barkhof F, Scheltens P, Stam CJ, Smith SM, Beckmann CF (2006). Consistent resting-state networks across healthy subjects. Proc Natl Acad Sci U S A 103:13848–13853.

De Martino F, Gentile F, Esposito F, Balsi M, Di Salle F, Goebel R, Formisano E (2007). Classification of fMRI independent components using IC-fingerprints and support vector machine classifiers. NeuroImage 34:177–194.

Duann JR, Jung TP, Kuo WJ, Yeh TC, Makeig S, Hsieh JC, Sejnowski TJ (2002). Single-trial variability in event-related BOLD signals. NeuroImage 15:823–835.

DuBois RM, Cohen MS (2000). Spatiotopic organization in human superior colliculus observed with fMRI. NeuroImage 12:63–70.

Esposito F, Scarabino T, Hyvarinen A, Himberg J, Formisano E, Comani S, Tedeschi G, Goebel R, Seifritz E, Di Salle F (2005). Independent component analysis of fMRI group studies by self-organizing clustering. NeuroImage 25:193–205.

Fischl B, Salat DH, van der Kouwe AJ, Makris N, Segonne F, Quinn BT, Dale AM (2004). Sequence-independent segmentation of magnetic resonance images. NeuroImage 23 Suppl 1:S69–84.

Formisano E, De Martino F, Bonte M, Goebel R (2008). "Who" is saying "what"? Brain-based decoding of human voice and speech. Science 322:970–973.

Formisano E, Esposito F, Kriegeskorte G, Tedeshi G, Di Salle F, Goebel R (2002). Spatial independent component analysis of functional magnetic resonance imaging time-series: characterization of the cortical components. Neurocomputing 49:241–254.

Fox MD, Raichle ME (2007). Spontaneous fluctuations in brain activity observed with functional magnetic resonance imaging. Nat Rev Neurosci 8:700–711.

Fox MD, Corbetta M, Snyder AZ, Vincent JL, Raichle ME (2006). Spontaneous neuronal activity distinguishes human dorsal and ventral attention systems. Proc Natl Acad Sci U S A 103:10046–10051.

Fox MD, Snyder AZ, Vincent JL, Corbetta M, Van Essen DC, Raichle ME (2005). The human brain is intrinsically organized into dynamic, anticorrelated functional networks. Proc Natl Acad Sci U S A 102:9673–9678.

Frackowiak RSJ, Friston KJ, Frith CD, Dolan RJ, Price CJ, Zeki S, Ashburner J, Penny W, eds (2004) Human Brain Function, 2 Edition: Elsevier Science (USA).

Frahm J, Bruhn H, Merboldt KD, Hanicke W (1992). Dynamic MR imaging of human brain oxygenation during rest and photic stimulation. J Magn Reson Imaging 2:501–505.

Fransson P (2006). How default is the default mode of brain function? Further evidence from intrinsic BOLD signal fluctuations. Neuropsychologia 44:2836–2845.

Friston KJ, Jezzard P, Turner R (1994). Analysis of Functional MRI Time-Series. Human Brain Mapping 1:153–171.

Friston KJ, Josephs O, Rees G, Turner R (1998a). Nonlinear event-related responses in fMRI. Magn Reson Med 39:41–52.

Friston KJ, Ashburner J, Frith CD, Poline J-B, Heather JD, Frackowiak RSJ (1995). Spatial Registration and Normalization of Images. Hum Brain Mapp 2:165–189.

Friston KJ, Fletcher P, Josephs O, Holmes A, Rugg MD, Turner R (1998b). Event-related fMRI: characterizing differential responses. NeuroImage 7:30–40.

Friston KJ, Glaser DE, Henson RN, Kiebel S, Phillips C, Ashburner J (2002). Classical and Bayesian inference in neuroimaging: applications. NeuroImage 16:484–512.

Glover GH, Li TQ, Ress D (2000). Image-based method for retrospective correction of physiological motion effects in fMRI: RETROICOR. Magn Reson Med 44:162–167.

Goebel R, Linden DE, Lanfermann H, Zanella FE, Singer W (1998). Functional imaging of mirror and inverse reading reveals separate coactivated networks for oculomotion and spatial transformations. Neuroreport 9:713–719.

Golland Y, Golland P, Bentin S, Malach R (2008). Data-driven clustering reveals a fundamental subdivision of the human cortex into two global systems. Neuropsychologia 46:540–553.

Golland Y, Bentin S, Gelbard H, Benjamini Y, Heller R, Nir Y, Hasson U, Malach R (2007). Extrinsic and intrinsic systems in the posterior cortex of the human brain revealed during natural sensory stimulation. Cereb Cortex 17:766–777.

Gray MA, Minati L, Harrison NA, Gianaros PJ, Napadow V, Critchley HD (2009). Physiological recordings: basic concepts and implementation during functional magnetic resonance imaging. NeuroImage 47:1105–1115.

Greicius MD, Krasnow B, Reiss AL, Menon V (2003). Functional connectivity in the resting brain: a network analysis of the default mode hypothesis. Proc Natl Acad Sci U S A 100:253–258.

Griffiths TD, Uppenkamp S, Johnsrude I, Josephs O, Patterson RD (2001). Encoding of the temporal regularity of sound in the human brainstem. Nat Neurosci 4:633–637.

Gu H, Engelien W, Feng H, Silbersweig DA, Stern E, Yang Y (2001). Mapping transient, randomly occurring neuropsychological events using independent component analysis. NeuroImage 14:1432–1443.

Guimaraes AR, Melcher JR, Talavage TM, Baker JR, Ledden P, Rosen BR, Kiang NY, Fullerton BC, Weisskoff RM (1998). Imaging subcortical auditory activity in humans. Hum Brain Mapp 6:33–41.

Gusnard DA, Raichle ME, Raichle ME (2001). Searching for a baseline: functional imaging and the resting human brain. Nat Rev Neurosci 2:685–694.

Haacke EM, Brown RW, Thompson MR, Venkatesan R. 1999. Magnetic Resonance Imaging Physical Principles and Sequence Design. John Wiley & Sons, Inc.

Hampson M, Peterson BS, Skudlarski P, Gatenby JC, Gore JC (2002). Detection of functional connectivity using temporal correlations in MR images. Hum Brain Mapp 15:247–262.

Hampson M, Olson IR, Leung HC, Skudlarski P, Gore JC (2004). Changes in functional connectivity of human MT/V5 with visual motion input. Neuroreport 15:1315–1319.

Hari R, Kujala MV (2009). Brain basis of human social interaction: from concepts to brain imaging. Physiol Rev 89:453–479.

Hasson U, Nusbaum HC, Small SL (2009a). Task-dependent organization of brain regions active during rest. Proc Natl Acad Sci U S A 106:10841–10846.

Hasson U, Nir Y, Levy I, Fuhrmann G, Malach R (2004). Intersubject synchronization of cortical activity during natural vision. Science 303:1634–1640.

Hasson U, Yang E, Vallines I, Heeger DJ, Rubin N (2008). A hierarchy of temporal receptive windows in human cortex. J Neurosci 28:2539–2550.

Hasson U, Avidan G, Gelbard H, Vallines I, Harel M, Minshew N, Behrmann M (2009b). Shared and idiosyncratic cortical activation patterns in autism revealed under continuous real-life viewing conditions. Autism Res 2:220–231.

Haynes JD, Rees G (2005). Predicting the orientation of invisible stimuli from activity in human primary visual cortex. Nat Neurosci 8:686–691.

Himberg J, Hyvarinen A, Esposito F (2004). Validating the independent components of neuroimaging time series via clustering and visualization. NeuroImage 22:1214–1222.

Hu D, Yan L, Liu Y, Zhou Z, Friston KJ, Tan C, Wu D (2005). Unified SPM-ICA for fMRI analysis. NeuroImage 25:746–755.

Hu X, Le TH, Parrish T, Erhard P (1995). Retrospective estimation and correction of physiological fluctuation in functional MRI. Magn Reson Med 34:201–212.

Huettel SA, Song AW, McCarthy G. 2005. Functional Magnetic Resonance Imaging. Sinauer Associates, Inc.

Hyvärinen A (1999). Fast and robust fixed-point algorithms for independent component analysis. IEEE Trans Neural Netw 10:626–634.

Hyvärinen A, Oja E (1997). A fast fixed-point algorithm for independent component analysis. Neural Computation 9:1483–1492.

Hyvärinen A, Oja E (2000). Independent component analysis: algorithms and applications. Neural Netw 13:411–430.

Josephs O, Turner R, Friston K (1997). Event-related fMRI. Human Brain Mapping 5:243–248.

Kamitani Y, Tong F (2005). Decoding the visual and subjective contents of the human brain. Nat Neurosci 8:679–685.

Kansaku K, Muraki S, Umeyama S, Nishimori Y, Kochiyama T, Yamane S, Kitazawa S (2005). Cortical activity in multiple motor areas during sequential finger movements: an application of independent component analysis. NeuroImage 28:669–681.

Kay KN, Naselaris T, Prenger RJ, Gallant JL (2008). Identifying natural images from human brain activity. Nature 452:352–355.

Krüger G, Glover GH (2001). Physiological noise in oxygenation-sensitive magnetic resonance imaging. Magn Reson Med 46:631–637.

Krumbholz K, Schonwiesner M, Rubsamen R, Zilles K, Fink GR, von Cramon DY (2005). Hierarchical processing of sound location and motion in the human brainstem and planum temporale. Eur J Neurosci 21:230–238.

Kwong KK, Belliveau JW, Chesler DA, Goldberg IE, Weisskoff RM, Poncelet BP, Kennedy DN, Hoppel BE, Cohen MS, Turner R, et al. (1992). Dynamic magnetic resonance imaging of human brain activity during primary sensory stimulation. Proc Natl Acad Sci U S A 89:5675–5679.

Langers DR (2009). Unbiased group-level statistical assessment of independent component maps by means of automated retrospective matching. Hum Brain Mapp.

Lauterbur PC (1973). Image Formation by Induced Local Interactions: Examples Employing Nuclear Magnetic Resonance. Nature 242:190–191.

Li YO, Adali T, Calhoun VD (2007). Estimating the number of independent components for functional magnetic resonance imaging data. Hum Brain Mapp 28:1251–1266.

Liang ZP, Lauterbur PC. 2000. Priciples of Magnetic Resonance Imaging A Signal Processing Perspective. New York: IEEE Press.

Ljunggren S (1983). A simple graphical representation of fourier-based imaging methods. Journal of Magnetic Resonance 54:338–343.

Logothetis NK (2002). The neural basis of the blood-oxygen-level-dependent functional magnetic resonance imaging signal. Philos Trans R Soc Lond B Biol Sci 357:1003–1037.

Logothetis NK (2003). The underpinnings of the BOLD functional magnetic resonance imaging signal. J Neurosci 23:3963–3971.

Logothetis NK, Pauls J, Augath M, Trinath T, Oeltermann A (2001). Neurophysiological investigation of the basis of the fMRI signal. Nature 412:150–157.

Lowe MJ, Mock BJ, Sorenson JA (1998). Functional connectivity in single and multislice echoplanar imaging using resting-state fluctuations. NeuroImage 7:119–132.

Ma L, Wang B, Chen X, Xiong J (2007). Detecting functional connectivity in the resting brain: a comparison between ICA and CCA. Magn Reson Imaging 25:47–56.

Malonek D, Grinvald A (1996). Interactions between electrical activity and cortical microcirculation revealed by imaging spectroscopy: implications for functional brain mapping. Science 272:551–554.

Mansfield P (1977). Multi-planar image formation using NMR spin echoes. Journal of Physics C: Solid State Physics 10:L55–L58.

McKeown MJ (2000). Detection of consistently task-related activations in fMRI data with hybrid independent component analysis. NeuroImage 11:24–35.

McKeown MJ, Makeig S, Brown GG, Jung TP, Kindermann SS, Bell AJ, Sejnowski TJ (1998). Analysis of fMRI data by blind separation into independent spatial components. Hum Brain Mapp 6:160–188.

Menon RS, Ogawa S, Hu X, Strupp JP, Anderson P, Ugurbil K (1995). BOLD based functional MRI at 4 Tesla includes a capillary bed contribution: echo-planar imaging correlates with previous optical imaging using intrinsic signals. Magn Reson Med 33:453–459.

Moritz CH, Rogers BP, Meyerand ME (2003). Power spectrum ranked independent component analysis of a periodic fMRI complex motor paradigm. Hum Brain Mapp 18:111–122.

Moritz CH, Carew JD, McMillan AB, Meyerand ME (2005). Independent component analysis applied to self-paced functional MR imaging paradigms. NeuroImage 25:181–192.

Napadow V, Dhond R, Conti G, Makris N, Brown EN, Barbieri R (2008). Brain correlates of autonomic modulation: combining heart rate variability with fMRI. NeuroImage 42:169–177.

Norman KA, Polyn SM, Detre GJ, Haxby JV (2006). Beyond mind-reading: multi-voxel pattern analysis of fMRI data. Trends Cogn Sci 10:424–430.

Ogawa S, Lee TM, Nayak AS, Glynn P (1990). Oxygenation-sensitive contrast in magnetic resonance image of rodent brain at high magnetic fields. Magn Reson Med 14:68–78.

Ogawa S, Tank DW, Menon R, Ellermann JM, Kim SG, Merkle H, Ugurbil K (1992). Intrinsic signal changes accompanying sensory stimulation: functional brain mapping with magnetic resonance imaging. Proc Natl Acad Sci U S A 89:5951–5955.

Pearson K (1901). On lines and planes of closest fit to systems of points in space. Philosophical Magazine 2:559–572.

Perlbarg V, Bellec P, Anton JL, Pelegrini-Issac M, Doyon J, Benali H (2007). CORSICA: correction of structured noise in fMRI by automatic identification of ICA components. Magn Reson Imaging 25:35–46.

Purcell EM, Torrey HC, Pound RV (1946). Resonance absorbtion by nuclear magnetic moments in a solid. Phys Rev 69:37.

Ramkumar P, Malinen S, Vartiainen M, Hlushchuk Y, Forss N, Kalso E, Hari R (2010) Hub maps reveal reduced resting-state connectivity of insular cortex in patients with chronic pain. In: 16th Annual Meeting of the Organization for Human Brain Mapping. Barcelona, Spain.

Rogers BP, Morgan VL, Newton AT, Gore JC (2007). Assessing functional connectivity in the human brain by fMRI. Magn Reson Imaging 25:1347–1357.

Schmithorst VJ, Holland SK (2004). Comparison of three methods for generating group statistical inferences from independent component analysis of functional magnetic resonance imaging data. J Magn Reson Imaging 19:365–368.

Svensen M, Kruggel F, Benali H (2002). ICA of fMRI group study data. NeuroImage 16:551–563.

Thomas CG, Harshman RA, Menon RS (2002). Noise reduction in BOLD-based fMRI using component analysis. NeuroImage 17:1521–1537.

Twieg DB (1983). The k-trajectory formulation of the NMR imaging process with applications in analysis and synthesis of imaging methods. Med Phys 10:610–621.

van de Ven VG, Formisano E, Prvulovic D, Roeder CH, Linden DE (2004). Functional connectivity as revealed by spatial independent component analysis of fMRI measurements during rest. Hum Brain Mapp 22:165–178.

Yang TT, Simmons AN, Matthews SC, Tapert SF, Bischoff-Grethe A, Frank GK, Arce E, Paulus MP (2007). Increased amygdala activation is related to heart rate during emotion processing in adolescent subjects. Neurosci Lett 428:109–114.

Yang Z, LaConte S, Weng X, Hu X (2008). Ranking and averaging independent component analysis by reproducibility (RAICAR). Hum Brain Mapp 29:711–725.

Ylipaavalniemi J, Savia E, Malinen S, Hari R, Vigario R, Kaski S (2009). Dependencies between stimuli and spatially independent fMRI sources: towards brain correlates of natural stimuli. NeuroImage 48:176–185.

Zarahn E, Aguirre GK, D'Esposito M (1997). Empirical analyses of BOLD fMRI statistics. I. Spatially unsmoothed data collected under null-hypothesis conditions. NeuroImage 5:179–197.

Zeng W, Qiu A, Chodkowski B, Pekar JJ (2009). Spatial and temporal reproducibility-based ranking of the independent components of BOLD fMRI data. NeuroImage 46:1041–1054.

Zhang WT, Mainero C, Kumar A, Wiggins CJ, Benner T, Purdon PL, Bolar DS, Kwong KK, Sorensen AG (2006). Strategies for improving the detection of fMRI activation in trigeminal pathways with cardiac gating. NeuroImage 31:1506–1512.

ISBN 978-952-60-3207-8
ISBN 978-952-60-3208-5 (PDF)
ISSN 1795-2239
ISSN 1795-4584 (PDF)